Geological Storage of CO_2: Sensitivity and Risk Analysis

Meisam Ashraf

Dissertation for the degree of Philosophiae Doctor (PhD)

Department of Mathematics
University of Bergen

April 2014

Scientific environment

This dissertation is submitted as a partial fulfillment of the requirements for the degree Doctor of Philosophy (PhD) at the University of Bergen. It is part of the project Mathematical Modeling and Risk Assessment of CO2 storage, MatMoRA, which was funded by the Norwegian Research Council of Norway, Statoil and Norske Shell under grant no. 178013/I30 and lead by Professor Helge Dahle at the Department of Mathematics, University of Bergen (UiB).

The working environment have been SINTEF-ICT in Oslo, CIPR in Bergen, and SIMTECH in Stuttgart. Professor Knut-Andreas Lie, chief scientist at SINTEF-ICT, has been the main adviser and Professor Jan M. Nordbotten at the Department of Mathematics, UiB, along with Halvor M. Nilsen, research scientist at SINTEF, have been co-advisers. With warm supports from Professor Rainer Helmig, head of Department of Hydromechanics and Modelling of Hydrosystems at Stuttgart University, last parts of the work is benefited from advices of professor Wolfgang Nowak, head of Stochastic Modelling of Hydrosystems, Dr. Sergey Oladyshkin, postdoctoral fellow at SIMTECH, and Professor Holger Class at Stuttgart University.

Acknowledgements

I dedicate this to my father.

With them the seed of Wisdom did I sow,
And with mine own hand wrought to make it grow;
And this was all the Harvest that I reap'd-
"I came like Water, and like Wind I go."

Omar Khayyam, 1048 – 1131.
Translated by Edward FitzGerald, 1809-1883.

My great thanks go to Knut-Andreas Lie who supported me throughout my study. I always enjoyed discussions with Halvor M. Nilsen, who initially was my only friend in Norway. Jan M. Nordbotten always inspired me in my works. Many thanks to Helge Dahle, who supported me during my stay in Bergen. I have enjoyed working with Segrey Oladyshkin, Wolfgang Nowak, and Holger Class while spending a semester in Stuttgart University. Special thanks go to friends and family who made my life more beautiful.

I would like also to acknowledge the sponsors of the MatMora project defined in the University of Bergen in partnership with SINTEF-ICT and the University of Stuttgart, and the German Research Foundation (DFG) for financial support of the project within the Cluster of Excellence in Simulation Technology (EXC310/1) at the University of Stuttgart.

Meisam Ashraf
Trondheim, November 2013

Abstract

Geological CO_2 storage has the potential to be a key technology for prevention of industrial CO_2 emission into the atmosphere. A successful storage operation requires safe geological structures with large storage capacity. The practicality of the technology is challenged by various operational concerns, ranging from site selection to long-term monitoring of the injected CO_2. The research in this report addresses the value of using sophisticated geological modeling to help in predicting storage performance.

In the first part, we investigate the significance of assessing the geological uncertainty and its consequences in site selection and the early stages of storage operations. This includes the injection period and the early migration time of the injected CO_2 plume. The extensive set of realistic geological realizations used in the analysis makes the key part of this research. Heterogeneity is modelled using the most influential geological parameters in a shallow-marine system, including aggradation angle, levels of barriers in the system, faults, lobosity, and progradation direction.

A typical injection scenario is simulated over 160 realizations and major flow responses are defined to measure the success of the early stages of CO_2 storage operations. These responses include the volume of trapped CO_2 by capillarity, dynamics of the plume in the medium, pressure responses, and the risk of leakage through a failure in the sealing cap-rock. The impact of geological uncertainty on these responses is investigated by comparing all cases for their performance. The results show large variations in the responses due to changing geological parameters. Among the main influential parameters are aggradation angle, progradation direction, and faults in the medium.

A sophisticated geological uncertainty study requires a large number of detailed simulations that are time-consuming and computationally costly. The second part of the research introduces a workflow that employs an approximating response surface method called arbitrary polynomial chaos (aPC). The aPC is fast and sophisticated enough to be used practically in the process of sensitivity analysis and uncertainty and risk assessment. We demonstrate the workflow by combining the aPC with a global sensitivity analysis technique, the Sobol indices, which is a variance-based method proven to be practical for complicated physical problems. Probabilistic uncertainty analysis is performed by applying the Monte Carlo process using the aPC. The results show that the aPC can be used successfully in an extensive geological uncertainty study.

List of papers

1. M. Ashraf, K.A. Lie, H.M. Nilsen and A. Skorstad, *"Impact of geological heterogeneity on early-stage CO_2 plume migration: Sensitivity study"*, Submitted to the Groundwater.

2. M. Ashraf, *"Impact of geological heterogeneity on early-stage CO_2 plume migration: Heterogeneity impact on pressure behavior"*, Submitted to the International Journal of Greenhouse Gas Control(IJGGC).

3. M. Ashraf, S. Oladyshkin, W. Nowak, *"Geological storage of CO_2: Application, feasibility and efficiency of global sensitivity analysis and risk assessment using the arbitrary polynomial chaos."* , Published in the International Journal of Greenhouse Gas Control (2013).

Contents

Scientific environment **i**

Acknowledgements **iii**

Abstract **v**

List of papers **vii**

1 Introduction **1**
1.1 Introduction . . . 2
1.2 Carbon storage . . . 3
1.3 Modeling procedure . . . 4
1.4 Uncertainty Sources . . . 6
1.5 Geological modeling . . . 7
1.5.1 Geological description . . . 7
1.5.2 Geological parameters . . . 10
1.6 Flow equations . . . 17
1.6.1 Single phase flow . . . 17
1.6.2 Two-phase flow . . . 19
1.7 Flow regimes . . . 24
1.7.1 Injection and early migration . . . 25
1.7.2 Long term migration . . . 27
1.8 Flow modeling . . . 28
1.8.1 Numerical scheme . . . 28
1.8.2 Flow scenarios . . . 31
1.8.3 Flow responses . . . 33
1.8.4 ECLIPSE input file . . . 44
1.9 Sensitivity and risk analysis . . . 47
1.9.1 Stochastic analysis . . . 47
1.9.2 Arbitrary polynomial chaos expansion . . . 47
1.9.3 Sensitivity analysis . . . 50
1.9.4 Risk analysis . . . 52
1.10 General summary . . . 52
1.10.1 Implementation of the work-flow . . . 53
1.10.2 Generic application of results . . . 53

2 Introduction to the papers **57**
2.1 Introduction . . . 58
2.2 Summary of papers . . . 58

3 Scientific results **63**
3.1 Impact of geological heterogeneity on early-stage CO_2 plume migration: Sensitivity study 65
3.2 Geological storage of CO_2: Heterogeneity impact on pressure behavior 91
3.3 Geological storage of CO_2: Application, feasibility and efficiency of global sensitivity analysis and risk assessment using the arbitrary polynomial chaos. 117

List of Figures

1.1 Green-house gases act like a blanket trapping part of the heat received from the sun. The low frequency radiations from the earth surface can not pass through the layer of green-house gas on the upper part of the atmosphere (shown by a red line in the figure). 3

1.2 The injected CO_2 (the yellow part) in the aquifer (the dark blue part) can be stored under the sealing geological structures (the brown part). 4

1.3 Modeling procedure diagram. The tasks are shown in yellow boxes and they fall in three main categories that are indicated by big cyan boxes. Arrows depict the flow of the procedure based on the sequence order of the tasks. 5

1.4 Schematic plots of heterogeneities in fluvial and beach depositions. The top view is illustrated in Figure (a) and Figure (b) shows the side view. The arrow in Figure (b) shows that the deposition mass is less heterogeneous than the fluvial systems. 8

1.5 Stratigraphic heterogeneity levels in lateral and vertical directions. Arrows direction indicates the increase in the heterogeneity level. Modified from [47]. 12

1.6 Fine grid perspective view. Colors depict rock types; see Figures 1.7 and 1.8. The geological structure is divided in two parts due to a faulting process. The eleveated part is considered in the study. 12

1.7 Perspective view of the rock type variations for a selected case mapped on a uniform grid. 13

1.8 Six different rock types used in modeling the stratigraphic heterogeneities. Compare with Figure 1.7 13

1.9 Histogram of lateral transmissibility for different facies in a selected case. Scales are logarithmic in units cP.m^3/day/bar. Only the x-axis is logarithmic. 14

1.10 Logarithmic of lateral transmissibility plotted for four layers in fine grid versus their representative layer in the coarse grid. The top view is plotted in all figures and units are cP.m^3/day/bar. 15

1.11 Top view illustration of faults used in the faulted grids. The fault plotted in red divides the medium in two parts (compare with Figure 1.6) and only the part below the red line in the top view is considered in the study. 15

1.12 Lobosity levels are defined based on the shoreline shape, which is caused by the interplay between fluvial and wave forces. From Figure (a) to (c) the system changes from wave to fluvial dominated. 16

1.13 Periodic floods and flactuations in fluvial system can result in shale draped surfaces. These surfaces act as barriers to flow in both vertical and horizontal directions. The barries are modeled in the SAIGUP study by modifiying the transmissibility of cells across the barrier (red surface in the plot). Barrier level variations are specified by areal coverage of zero transmissibility multipliers (indicated by blue color). 16

1.14 The change in the fluvial flux results in a shift in the depositional rock types from the river to the sea. The shift varies from very extensive in amount resulting in near horizontal layers of facies stocked on top of each other (low aggradation angles) to slight shifts resulting in near vertical rock type patterns (high aggradation angles). . . . 17

1.15 Techtonic activies in shallow marine systems can result in various orientations of river to sea depostions that is considered as progradation direction in the SAIGUP study. . . 17

1.16 The flow problem is solved over domain Ω that is bounded by Γ_i. The injection well is modeled as source point q. Geological heterogeneities can be in the form of discontinuity γ_i. 18
1.17 Permeability is an indication of how easy it is for the fluids to flow trough the medium. 19
1.18 In a multiphase system, phases wet the medium with diffrent degrees of preference. Wettability is defined by the angle between two phases' interface and the solid surface (Θ). The wetting phase makes an acute angle with the solid phase. Water is the wetting phase in this example. 20
1.19 The CO_2 (yellow parts) is the non-wetting phase and it flows through the water (blue parts) that wets the rock grains (brown parts) easier than CO_2. The cross section of the medium is illustrated here. 20
1.20 Relative permeability is an indication of how easy it is for the two phases to flow together through the medium. Relative permeability depends on the wettability of phases and the reltive volumes occupied by each phase (phase saturation). 21
1.21 Capillary pressure can be expressed as a function of wetting saturation. The plot shows a typical Van Genuchten curve for capillary pressure. The scale in the vertical axis is only for demonstration. For application, see for example [46] and [40]. 22
1.22 Capillary force is caused by the interaction of fluid phases with the pore walls. Capillary pressure is calculated from the force balance at the interface and depends on the curvature of the interface and the pore radius. 22
1.23 Water saturation (S_w) distribution in the capillary transition zone. In the hydrostatic equilibrium condition, phases exist at different depths with saturations that depend on the balance between capillary and gravity forces. 23
1.24 Flow regimes in geological CO_2 storage; (a) During injection, the main physical processes are the flow advection due to the imposed pressure by the injection, the gravity segregation due to the phase density differences, and the dissolution of CO_2 into water. (b) During the long-term CO_2 migration, the main physical processes in the medium are the gravity segregation, the molecular diffusion, the CO_2 dissolution in water, the water capillary imibibition, and the convection mixing due to gravity instabilities. . . . 29
1.25 Transmissibility between two cells a and b depends on the interface area perpendicular to the flow (A_{ab}) and transmissibilities between the center and the cell side within each cell (T_a and T_b). 30
1.26 Injection operation causes pressure increase near the well-bore. The red color in the figure demonstrates the regions with pressure build-up. The well-bore pressure is calculated by a relation that models the pressure distribution around the well. The black curve in the figure shows a schematic incline of the pressure near the injector. 30
1.27 In the models used for flow simulation, the top, bottom, and upper side boundaries are closed and the rest are open to the flow. Arrows point to the boundaries and their color indicates if the boundary is open (green) or closed (red). Colors on the grid show the depth of different locations. The injector location is depicted by a black line. 32
1.28 The aquifer can be connected to neighboring aquifer systems and the flow from those aquifers (red arrows in the plot) is modeled by imposing external pressure on the open sides of the model. The dotted box in the figure schematically indicates a domain considered for study. Aquifer layers outside the frame are considered external. The yellow color demonstrates the injected CO_2 in the aquifer. 34
1.29 Mobile and residual CO_2 volumes; the injected CO_2 plume travels upward within the geological formation and leaves behind a volume of residual CO_2 that is trapped due to capillarity. 34
1.30 We use a 2D Gaussian distribution for leakage probability on the cap-rock. 34

1.31 Transmissibility in the vertical direction for two selected cases. The left plots correspond to case A in Table 1.4, and the right plots belong to case B. Colors are in log scale and the scale in Figures (a) and (b) are powers of ten in cP.m^3/day/bar units. . . . 36
1.32 Transmissbility in the lateral direction for two selected cases. The left plots correspond to case A in Table 1.4, and the right plots belong to case B. Colors are in log scale and the scale in Figures (a) and (b) are powers of ten in cP.m^3/day/bar units. 37
1.33 CO_2 distribution at the end of injection for two selected cases. The left plots correspond to case A in Table 1.4, and the right plots belong to case B. 38
1.34 CO_2 distribution at the end of simulation for two selected cases. The left plots correspond to case A in Table 1.4, and the right plots belong to case B. 39
1.35 Flow sign in the X direction at the end of injection for two selected cases. The left plots correspond to case A in Table 1.4, and the right plots belong to case B. Red color corresponds to down-dip direction, blue to up-dip direction, and green represents the stagnant fluid. 40
1.36 Mobile CO_2 distribution at different times for two selected cases. Cases A and B are described in Table 1.4. Compare with Figures 1.31 and 1.32 for transmissibility values in different directions. Colors represent the same ranges shown in the colorbar. 41
1.37 Pressure development during injection and early migration. Pressure differences from hydrostatic pressure are shown for two selected cases. Values are in bar. Cases A and B are described in Table 1.4. Compare with Figures 1.31 and 1.32 for transmissibility values in different directions. 42
1.38 Marker codes used to plot the simulation results of all cases together. Aggradation is shown by different colors. Faults are shown by marker thickness; the thickest marker shows a case with close fault, medium thickness represents a case with open faults, and the thin markers indicate a case with no faults. All cases plotted in triples for the three degrees of faults. Therefor, plots contain 54 number of cases in the x-axis. The first 27 case numbers represent the up-dip progradation, and case numbers 28 to 54 have down-dip progradation. 43
1.39 Flowchart of workflow implemented in an automated procedure. 53

Chapter 1

Introduction

1.1 Introduction

"We won't have a society if we destroy the environment"
– Margaret Mead, American cultural anthropologist, 1901-1978

Climate changes resulting from CO_2 emissions caused by human have been shown in studies such as [36]. The underground sequestration of CO_2 produced from localized sources such as power-plants and oil and gas recovery sites is proposed as a possible solution to reduce the rate of CO_2 emission into the atmosphere [11, 35]. The technology required to inject CO_2 is similar to what is in use in the oil and gas and mining industry. However, there are two main challenges that are specific to carbon storage operations. First, the temporal and spatial scales in these problems are larger. Second, the risk of leakage of stored CO_2 up to the surface. The leakage can happen via natural features like fractures and faults or via man-made features such as leakage through ill-plugged wells and broken cap-rock due to high pressure imposed to the system during the injection operations is a major concern.

The main objectives of carbon storage operations are to maximize the storage volume and the volumetric injection rate, and to minimize the risk of leakage of the stored CO_2. The CO_2 storage operations require multidisciplinary collaborations. The work-flow from initial phases of a project until end of storage operations is divided between government and private sectors, research organizations and industry. In particular, it is the task of research community to investigate the safety of CO_2 sequestration and provide the methodology for CO_2 fate prediction [5].

Bachu [5] discusses a road-map of site selection for geological CO_2 sequestration. He defines the process in three steps: to assess the general suitability of the site, to perform an inventory study on source point, storage location, and operational transport issues, and finally to investigate the safety and assess the capacity of the storage. Safety and storage capacity issues are investigated from different perspectives such as immediate and ultimate results. As an example, the leakage through ill-plugged wells or fractures during the injection time is considered the immediate risk. However, leakage caused by plume migration long time after the injection and contamination to other aquifer systems are considered as ultimated risks.

To predict the fate of the injected CO_2, it is important to study the dynamics of flow in the storage medium. Study of flow dynamics includes quantification of acting forces in a geological heterogeneous medium as well as solving a complicated system of mathematical equations. It is convenient to replace the geological heterogeneous medium with an equivalent homogeneous medium to simplify the solution of the flow equations. However, proper modeling of geological heterogeneity is important in reservoir assessment and carbon storage studies [6, 19, 50, 51].

In this thesis, we report a series of studies performed within a PhD program. The work in this thesis is focusing on the fundamental uncertainty in geological description. The objective is to perform a sensitivity analysis on a set of geological parameters used to describe the geology of shallow-marine depositional systems. Although the focus is on a particular depositional system, the procedure can be implemented for other systems of interest. The work is reported in a series of papers.

The thesis is structured in three chapters. In the first chapter, we start by discussing the global warming and its causes, and the carbon storage as an interim proposed solution to mitigate the increasing level of industrial CO_2 emission to the atmosphere. Section 1.3 provides the work-flow of the works reported in the thesis. A literature overview is given in that section. A short discussion on different types of uncertainties in CO_2 storage operations is given in Section 1.4.

In Section 1.5, a detailed report on geological description is given, which includes information about the geological upscaling process. Flow equations for single-phase and two-phase flow problems are discussed in Section 1.6. In Section 1.7, various flow regimes occurring during geological storage

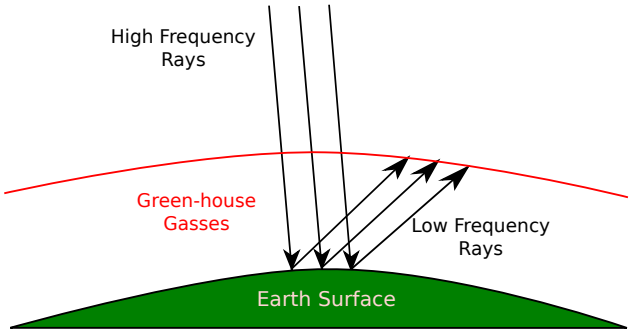

Figure 1.1: Green-house gases act like a blanket trapping part of the heat received from the sun. The low frequency radiations from the earth surface can not pass through the layer of green-house gas on the upper part of the atmosphere (shown by a red line in the figure).

of CO_2 are briefly described by discussing the force balance within the medium at different times. This section helps in evaluation of the simplifying physical assumptions taken in the study. For example, we discuss the circumstances under which the capillary pressure can be ignored in the study.

The introduction chapter continues in Section 1.8 by a discussion of flow simulation scenario and assumptions taken in the work. We use a set of flow responses to monitor the performance of the operation in a typical carbon storage process, with a special emphasis on the injection and early migration of CO_2 in the medium. Flow dynamics and a linear sensitivity analysis on the simulation results are discussed in this section.

Section 1.9 provides an overview of the techniques that can be used for fast flow simulations. We use a response surface method to evaluate the flow responses. This proxy model is then used in a global sensitivity analysis and Monte Carlo risk assessment process. At the end of this chapter, an overview of the work-flow and the limiting assumptions made in the study are discussed.

The second chapter consists of a summary of the included papers. A report on the comments and issues regarding each part of the research is given. In the last chapter, we present the scientific results of our studies.

1.2 Carbon storage

Causes of climate change are explained in numerous theories. Milankovich theory [29] relates the energy received from the sun to the cyclical variation of earth orbit around the sun, and earth rotation around its axis. The earth orbit changes eccentricity between circular and elliptical; This influences the distance between earth and sun, and in its peak it can reach to about 20% difference in the energy received from the sun. The second variation occurs in the rotation of earth around its plane axis. This rotation wobbles approximately every 13600 years and the summer solstice switches from June to January. Furthermore, a tilt variation of earth rotational axis happens approximately after every 41000 years. This can cause warmer winters and colder summers in high latitudes [29]. The solar radiation changes by a small amount of 0.1% over a 11 year cycle. On the scale of tens to thousands of years, variations in the earth orbit result in seasonal changes, which in the past caused glacial and inter-glacial cycles.

The theory of green house effect relates the earth climatic change to the fact that the long wave radiation from earth back to atmosphere is absorbed by the green-house gases, mainly carbon dioxide, water vapor, and methane existing in the atmosphere. This results in trapping of heat energy and an increase in atmosphere temperature level (Figure 1.1) [29].

Human manipulations in the nature has led to approximately 100 ppm increase in carbon dioxide

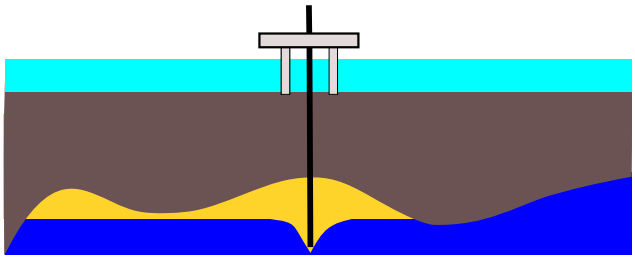

Figure 1.2: The injected CO_2 (the yellow part) in the aquifer (the dark blue part) can be stored under the sealing geological structures (the brown part).

level in the atmosphere. Most scientists believe that we are already experiencing the global warming due to green house effects. The IPCC Second Assessment report states that the observed warming trend since the late 19^{th} century is unlikely to be entirely natural in origin and is partly due to anthropogenic causes [14].

Carbon capture and storage (CCS) has received major attention in the industry and the scientific communities. According to the International Energy Agency (IEA), the cost of mitigating climate change by 2050 is estimated to be 70% higher without implementing CCS [39].

The CCS is considered as an interim solution, because it is valid due to fossil fuel consumption, and the long term strategy of replacing fossil fuel with renewable energy will terminate the validity of the CCS. Therefore, initiating CCS has to be conducted in a reasonable fashion such that it does not slow down the research for renewable energy. Another concern regarding CCS is the acceleration of coal and fossil fuel consumption with the excuse of availability of CCS technology.

Sequestration of CO_2 at the ocean floor and also in deep underground aquifers (Figure 1.2) are some of the available options for permanent storage of CO_2. The geological sequestration is considered an attractive solution because of availability of large storage capacity in the aquifers. Nevertheless, this alternative is not free from economical, social and industrial concerns.

In the last decades, the scientific community has been putting efforts into convincing the public regarding the feasibility of CO_2 storage operations. Social awareness is the first step in public agreement regarding the geological CO_2 storage. The EU has conducted a survey to assess the public awareness in 12 European states, which is published in the Eurobarometer report in May 2011. People's awareness of climate change and its causes, and their acceptance of the methods to avoid or mitigate the problems, in particular the CCS technology, was examined in the survey. The majority of European participants are either fairly or very well informed about causes and consequences of climate change. However, the awareness of the CCS among the European respondents was low. Two third of the participants in the survey have had not heard about the CCS.

The same survey suggests that the overall trust in Europe in the sources of information regarding the CCS is best in universities and other scientific institutions. Governments are investing in research, not only to move toward industrialization of the CCS, but also to make it well received by public. This highlights the importance of researching the storage of CO_2 and the way it is needed both for industrial and social concerns.

1.3 Modeling procedure

Predicting the fate of CO_2 storage involves identification and quantification of the relevant uncertainties and risk assessment process. The procedure starts with a geological description and continues with modeling of flow in geological formations. After constructing a deterministic flow model, the stochastic nature of the problem is analyzed by studying the variation in the model outcome due to uncertainties in the system.

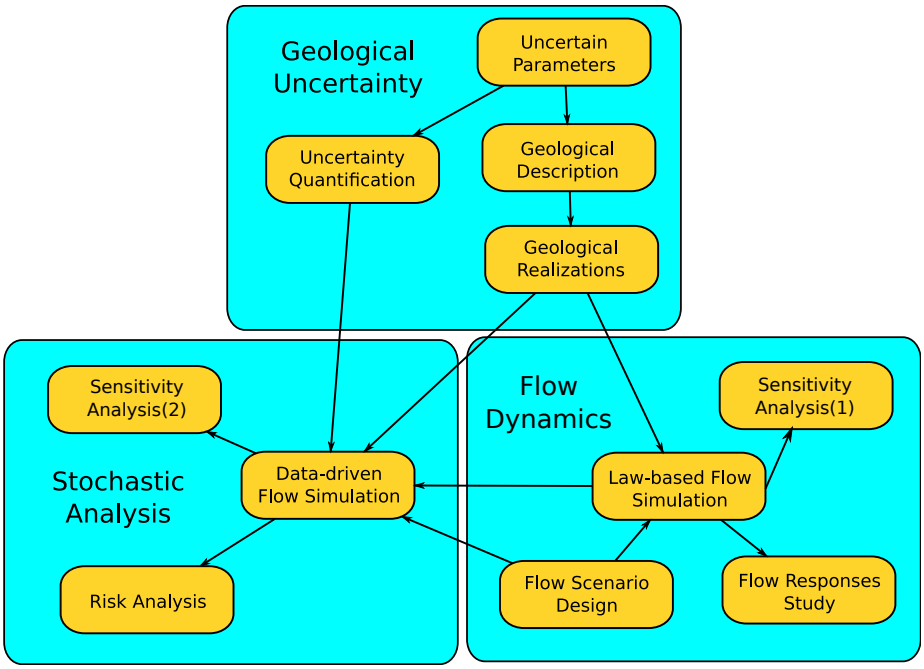

Figure 1.3: Modeling procedure diagram. The tasks are shown in yellow boxes and they fall in three main categories that are indicated by big cyan boxes. Arrows depict the flow of the procedure based on the sequence order of the tasks.

Figure 1.3 shows the modeling work-flow implemented in this thesis. The steps are categorized in three parts: geological uncertainty, flow dynamics, and stochastic analysis. The relations between the steps are plotted by arrows in the flow-chart. In this section, we briefly describe each step. More details will follow in the next sections.

Uncertain parameters: In the first step, we identify the uncertain parameters of the model to study their influence on the modeling outcome. It is possible that our knowledge of model sensitivity to the parameters is limited. In a conservative approach we choose a larger number of parameters and by doing a primary sensitivity analysis with a fast technique, we filter out the important parameters. Herein, the focus is on geological parameters that are determined to be the most influential source of geological uncertainty for shallow-marine environments [38].

Uncertainty quantification: After identification of the uncertain geological parameters, we assign a likelihood value to each of the parameters. It is hardly possible to have a unique likelihood profile that applies to every geological location. Thus, we note that probabilities of existence for an uncertain geological feature can change from place to place. The uncertainty enters the modeling in the form of parameter frequency histograms. The conventional practice is to consider an analytical distribution function to be assigned to the parameters. However, the sampling procedure normally ends in scarce frequency histograms that are difficult to fit into a unique analytical distribution function.

Geological description: Geological uncertainty study is normally done by series of runs to measure the sensitivity of the model to the parameter variations. Results are valid, only if the geology used in the work-flow is representative of reality. The process of geological description results in a large number of realizations to be used in the next steps of the study. Herein, we will use a set of equiprobable geological realizations of a shallow-marine reservoir.

Flow scenario design: Herein we define the initial and boundary conditions of the CO_2 injection problem. Also, we specify the injection scenarios. Simplifying physical assumptions will be taken here. Each scenario is implemented for all geological realizations.

Law-based flow modeling: After defining the injection problem, we simulate the flow dynamics in the available realizations. We use a two-phase flow model and a standard commercial simulator.

Data-driven flow modeling: Modeling the flow dynamics via formulation of physical laws normally results in complicated equations with many degrees of freedom. The computational cost of solving these equations is high, in particular for uncertainty related studies that require a large number of simulations to cover the variation in the uncertain parameters. So called data-driven methods, are mathematical functions that are specified by correlating a set of unknown flow attributes to their corresponding uncertain parameter values. These methods need to be tuned by a law-based method before employment. Because these methods are designed to be only dependent on the uncertain parameters, they are normally low in computational costs. However, they may exhibit the pitfall of not following the physical rules and in some cases produce unrealistic results.

Flow responses study: Once the simulation results are obtained from the flow modeling procedure, it is possible to calculate the important flow responses from simulation results. The fate of carbon storage and assessment of the operations can be inferred from these responses. Storage capacity, injection rate, and leakage risk are evaluated from flow responses. Responses include pressure distribution over time. CO_2 plume development, and other quantities describing the dynamics of flow.

Sensitivity and risk analysis: The sensitivity analysis is performed in two ways: In the first method, we use three-dimensional, two-phase flow simulations on all realizations available for demonstrating the geological variability. In the second method, we employ an approximating polynomial to perform global sensitivity analysis and stochastic uncertainty studies. Using a relatively fast data-driven method, we perform a Monte Carlo process on 10000 simulation cases.

1.4 Uncertainty Sources

Sources of uncertainty can exist in every part of the CO_2 storage modeling process. Herein, we describe each of the possible contributions to the uncertainty in the modeling within various parts.

Uncertainty in physical modeling: We may ignore some phenomena during the physical modeling of CO_2 storage that can be influential in the flow behavior. This can happen due to lack of awareness of the phenomena or by underestimating the significance of it. For example, we may ignore the heat exchange within the system, assuming that heat transfer does not play an important role in the flow performance. If some parameters in the modeling are sensitive to the heat and change by temperature variations, then the assumption to ignore heat transfer effect can introduce considerable bias in the outcome of the modeling.

Mathematical formulation and numerical approximation: Modeling CO_2 injection and migration in a realistic geological formation results in a complicated mathematical system that in most of the cases can not be solved analytically. The numerical approach to approximate the original mathematical system, normally introduces errors in the results. Mathematical analysis can help in estimating the error or its order, but it might not be doable for complicated models.

A specified physical problem can be formulated mathematically in more than one way. The choice of primary unknowns to be found can change the mathematical form and nature of the equations. Degrees of non-linearity and coupling between unknowns in the equations can vary in different formulations.

Geological uncertainty: The high costs of data acquisition and technical limitations introduce a huge amount of geological uncertainties in CO_2 storage modeling. The injected CO_2 may travel in a large spatial scale. Geological characterization of such a large medium is a big challenge.

User introduced uncertainty: These type of uncertainties are caused by the errors introduced by the user for his/her biased choice of modeling tools and interpretation of modeling results.

1.5 Geological modeling

The central part of a successful CO_2 storage modeling is to provide aquifer models that depict the geological heterogeneity in a realistic manner. This requires having an inclusive understanding about model sensitivity with respect to different geological parameters and quantifications of geological uncertainty and its impact on the process.

The conventional practice of geological modeling includes using geostatistical models. It is possible that two different heterogeneity patterns produce the same geostatistical model, as discussed by Caers [12]. Therefore, a geostatistical model does not represent a unique reservoir image and if we do not include additive information in the process, we may end-up with an unrealistic heterogeneity texture[12, 19]. The primary attention in our work has been on this issue and to provide a more realistic way of geological uncertainty analysis for CO_2 sequestration by including information of geological features and textures in the process.

1.5.1 Geological description

Geological storage of CO_2 requires large accommodation of subsurface volumes. Only sedimentary basins, which hold relative large pore volumes, are generally suitable for this mean. However, not all sedimentary basins are similarly appropriate for CO_2 sequestration.

Convergent basins along active tectonic areas pose a higher risk of CO_2 leakage due to volcanism, earthquakes, and active faults. Divergent basins located on the stable lithosphere are much less prone to earthquakes or other catastrophic event that can lead to accidental release of large CO_2 quantities. Therefore, specific considerations must be done in selecting site locations with respect to security of subsurface storage.

Sedimentary basins are composed of various lithological facies. Stratigraphic architecture and sandbody geometry control the capacity and effectiveness of CO_2 sequestration. As a result of various tectonic depositional and erosional process, low and high permeability rocks are accumulated on top of each other and can form stratigraphic flow-path leading to various directions and speed of subsurface flow. Three types of formations can be characterized as aquifers, aquitards, and aquicludes.

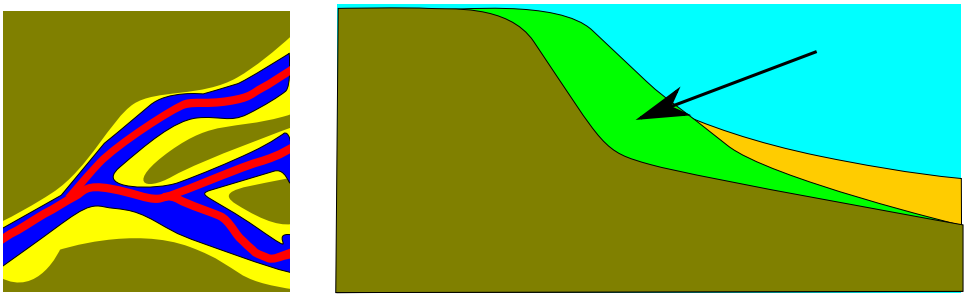

(a) Fluvial depositional system. (b) Beach depositional system.

Figure 1.4: Schematic plots of heterogeneities in fluvial and beach depositions. The top view is illustrated in Figure (a) and Figure (b) shows the side view. The arrow in Figure (b) shows that the deposition mass is less heterogeneous than the fluvial systems.

Aquifers are high permeability strata that provide major beddings for flow transport. Good rock quality in continuous sandbodies allow for efficient CO_2 storage in an acceptable capacity volumes. Aquitards are made of low permeability strata that provide beddings with orders of magnitude slower flow than aquifers. Layers of aquifers and aquitards are formed by thick accumulation of sediments that undergo burial, compaction, lithification, and uplift over millions of years. They can be covered by aquicludes, which are evaporative beds that are impervious to fluid flow. Typical seal rocks include, from most ductile to most brittle: salt, anhydrite, krogen-rich shales, dense mudstone, tightly cemented sandstones, anhydrite-filled dolomite, carbonate, or silica-cemented sandstones, and cherts.

Aquifer pressure is normally close to hydrostatic, because the conductivity within the medium allows for pressure equilibrium over long time. High pressurized compartments can exist in highly sealed structures. The pressure of the sedimentary basin has a significant impact on its suitability for CO_2 storage [5]. Trapping mechanism for CO_2 can happen due to stratigraphic or structural traps. Stratigraphic trapping is primarily controlled by the geometry of depositional facies and sand body continuity. These factors control the permeability distribution within the medium that controls the efficiency of injection and storage of CO_2. Structural heterogeneity factors include faults, folds, and fracture intensity. The dip angle of formation layers control the buoyancy forces that govern CO_2 plume migration along the conductive layers. Fractures can enhance the mobility of the plume and sealing faults can provide structural traps for long-term CO_2 storage. Anticline structures can also be permanent traps for stored CO_2.

Depositional environment varies from fluvial to marine systems. The texture and degree of sandiness of beach deposits are functions of the shore profile, typically consisting of a gently sloping formation layering in a transition from near shore to deep offshore. Deposits range from sandy, coarse grain structure near the shore, to muddy, burrowed, fine grained sand in the lower offshore. High energy near the shore that is a result of interplay between wave, fluvial, and tidal forces, filters out the larger grains in the deposition.

Therefore, formations closer to the shore contain large continuous sand bodies that have good quality rock. This is the reason for shallow-marine systems to be appropriate traps for hydrocarbons and analogously, good candidates for CO_2 storage.

The beach facies normally are homogeneous rocks with internal heterogeneity due to tidal systems. In contrast, mixed-load fluvial deposits that contain both mud and sand are more heterogeneous than beach systems. The presence of numerous mud drapes as a result of periodic floods, serves as barriers to fluid flow. Heterogeneity in the fluvial systems exist on multiple scales, from small-scale variations of rock type near the river bed, to the large-scale heterogeneity in fluvial channel-fill sandstones and over-bank deposits. Heterogeneity also occurs within these systems in the form of muddy abandoned channel-fill deposits.

In theory, we prefer a medium that allows for more lateral movement to overcome the buoyancy bypassing of the flow. Heterogeneity in the vertical direction, such as shale inter-bed barriers can serve for enhancing the lateral flow and disperse the flow in the lateral direction. Structural heterogeneities can have a similar impact. In addition, splitting a large plume into smaller plumes lowers the risk of leakage of huge CO_2 amounts via potential breakings in the integrity of the sealing barriers or abandoned wells.

CO_2 injectivity is related to sequestration capacity and effectiveness, and can be defined by the conductive cross-sectional area. Stratigraphic factors that enhance injectivity are high permeability and injection interval thickness. In addition, the lateral permeability architecture can influence the injectivity quality. The lower the injectivity is, the higher will be the pressure buildup in the medium due to injection.

Over the last two decades, there have been a large number of studies concerning the subsurface storage of CO_2. Several authors investigate the efficiency of geological CO_2 storage based on regional data in a specific site location. A case study from the Texas Gulf Coast [37] investigates the sequestration capacity and efficiency in accordance to the geological heterogeneity. The study performs a site-scale assessment of brine aquifers for geological CO_2 sequestration. Injection is considered in the Frio formation which is a sandstone-rich, high quality rock, overlain by thick, regionally extensive shale in the upper Texas Gulf Coast. Migration of CO_2 during injection (20 years), and post-injection (40 years) is studied in different geological realizations. The heterogeneity represented by stochastic modeling of geological sediments. Structural heterogeneity is modeled by layers dip angle and faults at different locations. Six models are made based on regional available geological information. The study shows that in a homogeneous rock volume, CO_2 flow paths are dominated by buoyancy, bypassing much of the lateral rock volume. If the permeable rock is inter-bedded with multiple low permeability layers, the flow paths are dispersed, enhancing the lateral movements of CO_2 and allowing for larger percentage of contact with rock volume. The study suggests that dip angle enhances buoyancy forces and decreases storage capacity, while compartmentalization by faulting appears to increase sequestration capacity at the cost of increased pressure, and consequently, increased risk of CO_2 leakage.

A number of pilot sites are established worldwide to test the large-scale injection of CO_2 in the subsurface formation. The In Salah project [60] in Algeria is an industrial-scale injection project into a fracture-influenced, matrix-dominated sandstone formation. The reservoir matrix comprises tidal deltaic sandstone. The project benefits from relatively high level of data acquisition: wireline and LWD well logs, image logs and production and geophysical monitoring [60]. In addition, the most valuable monitoring method has been the use of satellite airborne radar above the injection well. Also, chemical tracers are used in the injected CO_2 to differentiate the natural CO_2 in place from the injected volumes, when the CO_2 breaks through other wells. The detailed analysis highlights the geological controls on the movement and dispersion of CO_2 plumes. The injection is performed via a horizontal well perpendicular to the geomechanical stress field and the faults present in the domain. This, along with the fracture network, enhance the plume migration, which is about three times faster than the flow in a homogeneous domain. Results from In Salah illustrate the value of reducing geological uncertainty by employing sufficient logging tools and monitoring techniques.

The CO_2-SINK project at Ketzin Germany [28] is another pilot site for practicing subsurface CO_2 injection. The injection is performed in the Stuttgart formation that is geologically heterogeneous within an anticline structure. The Stuttgart formation is made of sandy channel facies of good rock quality alternate with muddy flood-plain-facies. A thick cap-rock section covers the Stuttgart formation.

Practically, including all details of every scale into a flow simulation model is impossible. Various simplifications have been made to account for heterogeneities in modeling. Some earlier studies consider two dimensional modeling, with homogeneous or geostatistically populated permeabilities. The study in [45] simulates an escape rate of CO_2 in a homogeneous medium similar to Utsira formation in Norway. By changing the horizontal permeability, they demonstrate that most of the injected CO_2 volume accumulates in a fine layer beneath the cap-rock due to buoyancy forces in the long-term CO_2 migration process. However, this study assumes no vertical heterogeneities. A layered heterogeneity

is examined in [68]. They used a log normal distribution of permeability in a simplified two dimensional grid to account for viscous and gravity forces. Results suggest that the sweep efficiency of CO_2 in the porous medium is low, and heterogeneity, in particular the vertical transmissibility, can have a big impact on the storage efficiency.

To examine the impact that the geological heterogeneity degree can have on the CO_2 sequestration modeling, [26] constructed a suite of three-dimensional simulation models, with varying net to gross ratios. A radial variogram, with a shale length of 300 m, was used to populate five models of varying degrees of net-sand-to-gross-shale ratios. The models were up-scaled, using flow-based methods, to make the computation feasible. The study concludes that formations containing shale barriers are effective in containing an injected CO_2 plume within the formation and that heterogeneity serves to limit the reliance of the formation seal as the only mechanism for containment.

1.5.2 Geological parameters

From the flow modeling perspective, sources of geological uncertainty can manifest themselves in the rock parameters, such as permeability and porosity, that go in the flow equation . However, to represent the geological uncertainty, it is not enough to randomize these parameters. This approach might work in simple geological models, but it can fail to give plausible results for the realistic heterogeneous problems with uncertain structural and depositional descriptions.

In response to the EU priorities of reducing time to first oil and of improving overall hydrocarbon recovery efficiency, the interdisciplinary SAIGUP study was initiated to increase the understanding of the influence of geological uncertainties in oil field recoveries. SAIGUP stands for 'sensitivity analysis of the impact of geological uncertainties on production forecasting in clastic hydrocarbon reservoirs'. The context in SAIGUP is defined for shallow-marine depositional systems. The main objective of the SAIGUP project has been to perform a quantitative sensitivity analysis to measure the impact of sedimentological and structural variations within geological descriptions on oilfield recovery estimates [38, 47, 48]. Herein, we will use six different rock types to investigate the impact of geological heterogeneities on CO_2 sequestration. The rock properties within each facies are populated based on real data. Variations are considered in a horizontal-vertical matrix in three levels of heterogeneities, low, medium, and high, as illustrated in Figure 1.5. The design focused on special considerations; for example, making complex enough heterogeneities to be a plausible representative of realistic models, and producing large enough number of realizations with sufficient overlapping to be able to perform a quantitative sensitivity analysis.

Sedimentological variability is modeled in small and large scales and combined to provide realistic variations of reservoir heterogeneities. All models are considered in a progradational sedimentary environment. A regular grid is used for all of the realizations in two gridding resolutions, fine and coarse, and the total bulk volume is the same in all cases. Each geological realization contains about 1.5 million cells in the fine model. Figure 1.6 shows the fine grid model for a selected realization with medium level of heterogeneity. A major fault in the model breaks the structure and makes large vertical depth difference in the two parts of the model (from about 1500 m to 3000 m). Thickness of the model is much smaller than these depth differences. To make it easier to see the property variations on the grid in the vertical direction, we map the properties on a flat uniform geometry (Figure 1.7).

Figure 1.8 shows the spatial distribution of the six modelled facies in the selected realization, and Figure 1.9 shows the histogram of lateral transmissibility within each facies in the logarithmic scale. Each facies is modeled separately in some levels of upscaling starting from the lamina scales, before populating on the fine grid. Flow based upscaling techniques are used, and the suitability of the methods depends on the balance of forces. When the medium is conductive due to high permeability, the viscous dominated steady state method is used. In the rocks with lower transmissibility where the capillary forces are dominant, the capillary equilibrium is assumed [47].

On the last step, the fine populated grid is mapped on to the coarse grid that is to be used for the flow solver. Since the grid size in the fine model is too expensive computationally for flow simulations,

Table 1.1: Grid specifications for fine and coarse scales in the SAIGUP modeling process.

Parameter	Fine Scale	Coarse Scale
Number of cells in the x direction	80	40
Number of cells in the y direction	240	120
Number of cells in the z direction	80	20
Number of total cells	1,500,000	96,000
Number of active cells	1,500,000	79,000
Model x dimension	3 *km*	3 *km*
Model y dimension	9 *km*	9 *km*
Model z dimension	80 *m*	80 *m*
Cell x dimension	37.5 *m*	75 *m*
Cell y dimension	37.5 *m*	75 *m*
Cell z dimension	1 *m*	4 *m*

the lateral dimension is doubled in each cell while every four layers are lumped into one layer in the vertical direction. Figure 1.10 shows the top view of lateral transmissibility in logarithmic scale for four consecutive layers of a selected case, and their corresponding upscaled layer in the coarse grid. Table 1.1 shows the grid specifications in the coarse and fine SAIGUP models.

A detailed discussion about the upscaling of the sedimentological and structural parameters for SAIGUP simulation models can be found at [47].

Structural aspects are modeled via fault modeling. Within the SAIGIP setup, faults are considered with different levels of intensity, orientation, and transmissibility. The orientations may vary in both lateral directions, and we consider a grid that contains faults in both directions (Figure 1.11).

Although these models were designed to study the impact of geological heterogeneity on oil recovery, they may also be used to model a scenario in which CO_2 is injected into an abandoned reservoir. Therefore, we have selected five parameters from the setup and varied these parameters by combining different levels for our CO_2 storage study. These features are lobosity, barriers, aggradation angle, progradation, and fault. In the following, we describe each feature briefly.

Lobosity: Lobosity is a metric for describing the interplay between fluvial and wave processes in a shallow-marine depositional system. As a river enters the mouth of the sea, the shore-line shapes where the river flux crashes with the waves from sea. The balance between the sediment supply from rivers and the available accommodation space in the shallow sea defines the shore-line shape. Sea waves smear out the shore-line, while fluvial flux from river makes branches into the sea. Less wave effect produces more pronounced lobe shapes around the river entrance into the sea.

The channels made into the sea mouth by fluvial supplies contain good quality rocks with relatively higher porosity and permeability. Poor quality rock types are located between the conductive branches. Reservoir quality decreases with distance from the shore-face. Lobosity variation can influence the CO_2 injection operation and plume distribution in the aquifer. In this study, models of three levels of lobosity are used: flat shoreline, one lobe and two lobes, see Fig. 1.12.

Barriers: Barriers are mud-draped surfaces sitting between reservoir sections that are caused by periodic floods in a shallow-marine depositional system. Mud-drapes extend in both vertical and lateral directions and are potential significant barriers to flow. In the SAIGUP domain used here, these barriers were modeled by defining areas between layers with zero transmissibility multipliers. This areal coverage was designed in three levels: low (10%), medium (50%), and high (90%). We use the same variations in this study, see Fig. 1.13.

Aggradation angle: In shallow-marine systems, the sediment supply from rivers deposits in a spectrum of large size grains in the land side toward fine grains deep in the basin. Amount of deposition

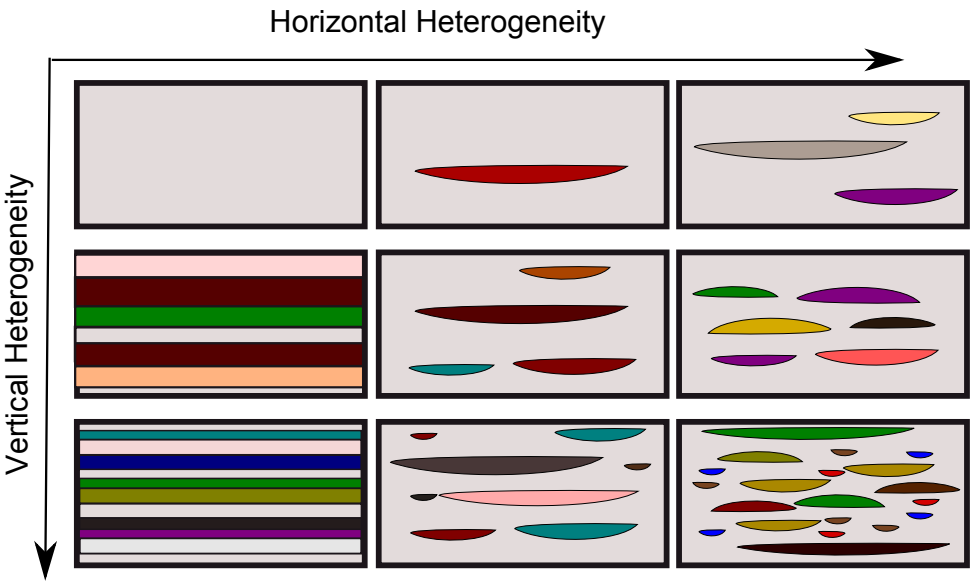

Figure 1.5: Stratigraphic heterogeneity levels in lateral and vertical directions. Arrows direction indicates the increase in the heterogeneity level. Modified from [47].

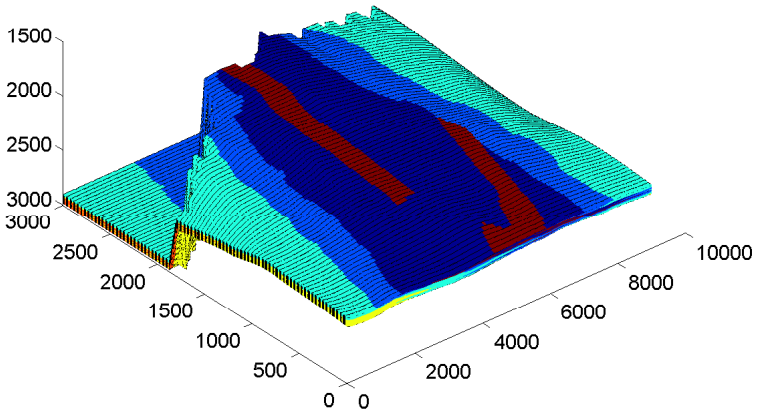

Figure 1.6: Fine grid perspective view. Colors depict rock types; see Figures 1.7 and 1.8. The geological structure is divided in two parts due to a faulting process. The eleveated part is considered in the study.

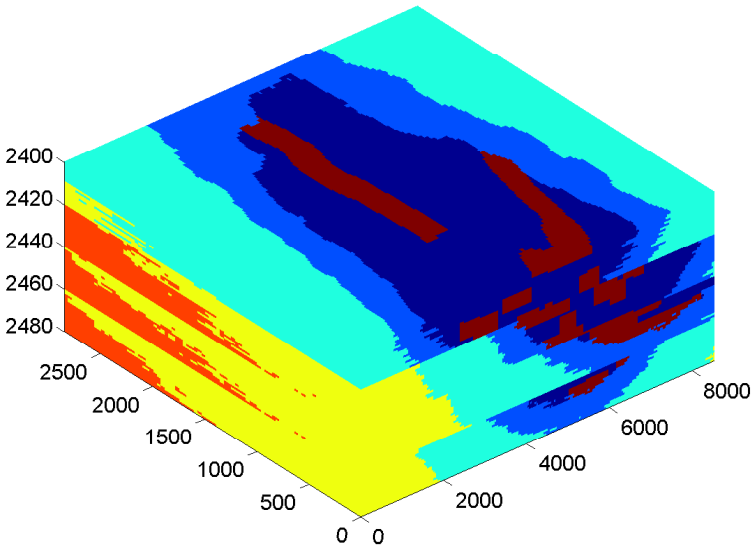

Figure 1.7: Perspective view of the rock type variations for a selected case mapped on a uniform grid.

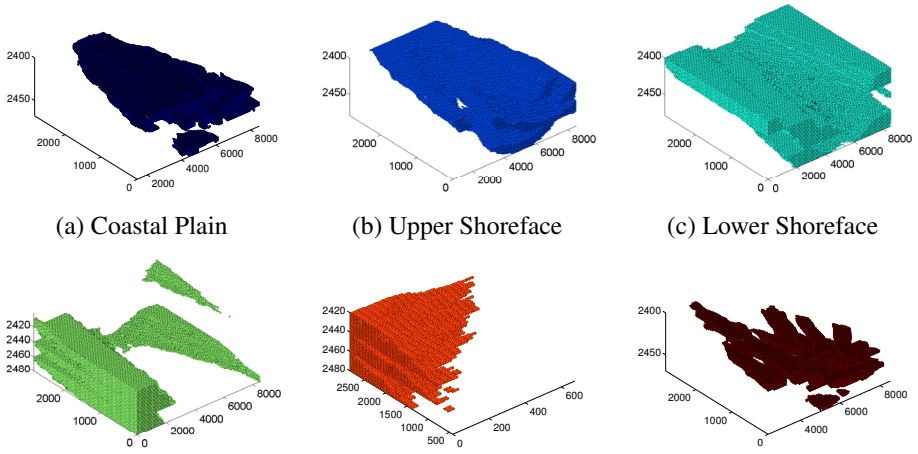

(a) Coastal Plain (b) Upper Shoreface (c) Lower Shoreface

(d) Offshore Transition (e) Offshore (f) Channels

Figure 1.8: Six different rock types used in modeling the stratigraphic heterogeneities. Compare with Figure 1.7

.

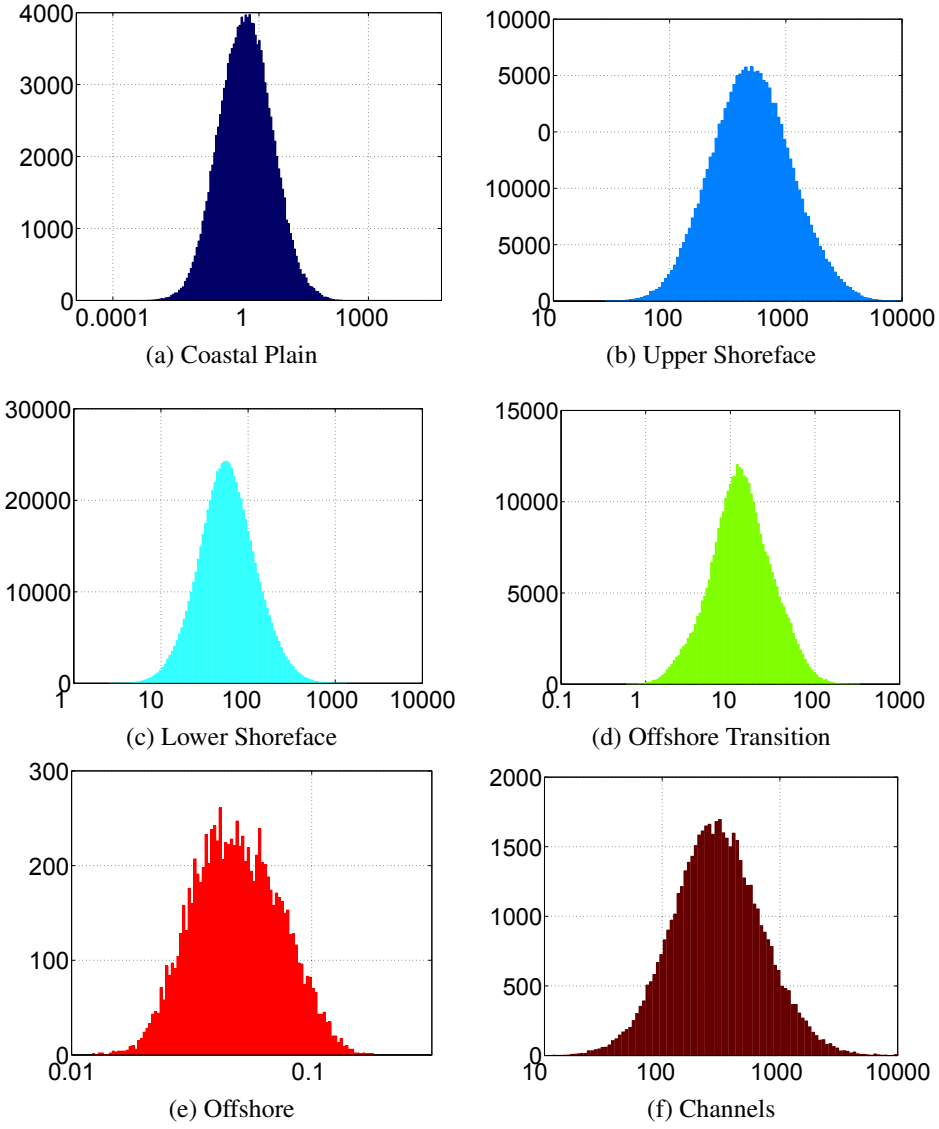

(a) Coastal Plain (b) Upper Shoreface

(c) Lower Shoreface (d) Offshore Transition

(e) Offshore (f) Channels

Figure 1.9: Histogram of lateral transmissibility for different facies in a selected case. Scales are logarithmic in units cP.m^3/day/bar. Only the x-axis is logarithmic.

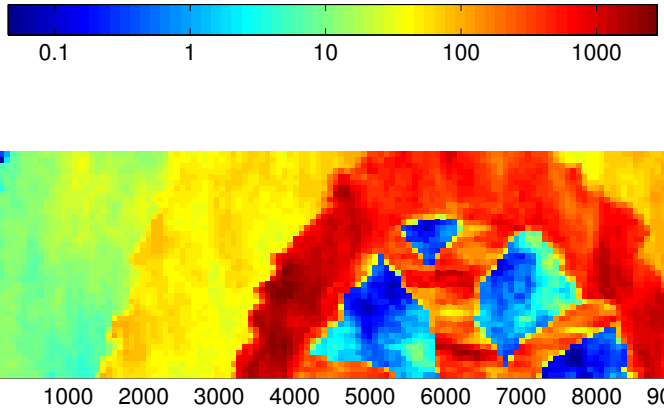

(a) Coarse grid.

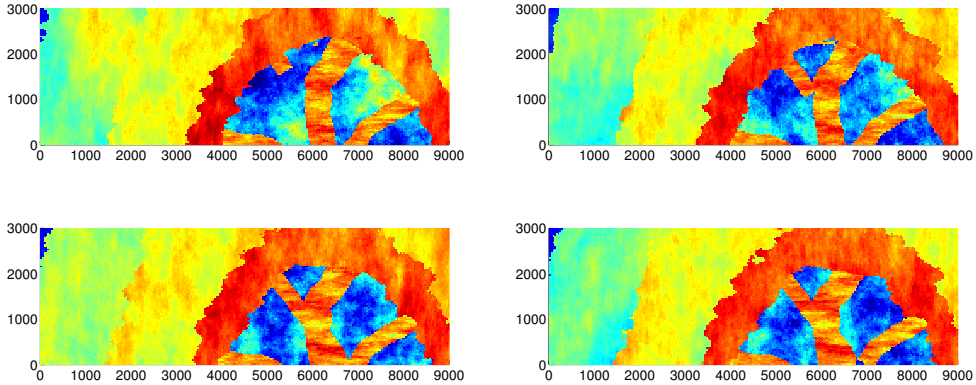

(b) Fine grid.

Figure 1.10: Logarithmic of lateral transmissibility plotted for four layers in fine grid versus their representative layer in the coarse grid. The top view is plotted in all figures and units are cP.m^3/day/bar.

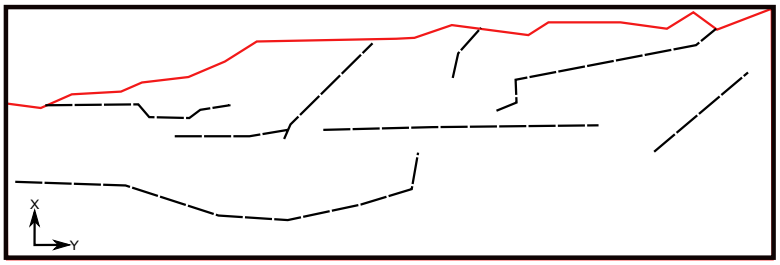

Figure 1.11: Top view illustration of faults used in the faulted grids. The fault plotted in red divides the medium in two parts (compare with Figure 1.6) and only the part below the red line in the top view is considered in the study.

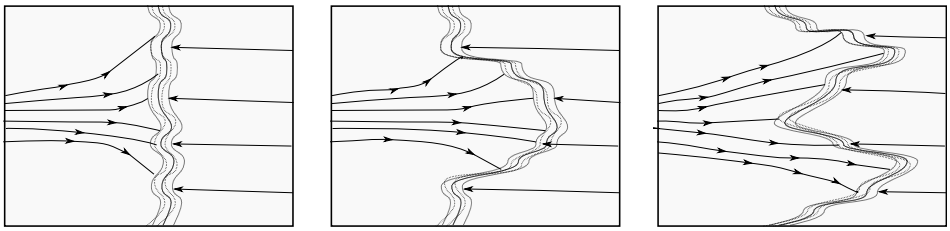

(a) Flat shoreface. (b) One lobe shoreface. (c) Two lobe shoreface.

Figure 1.12: Lobosity levels are defined based on the shoreline shape, which is caused by the interplay between fluvial and wave forces. From Figure (a) to (c) the system changes from wave to fluvial dominated.

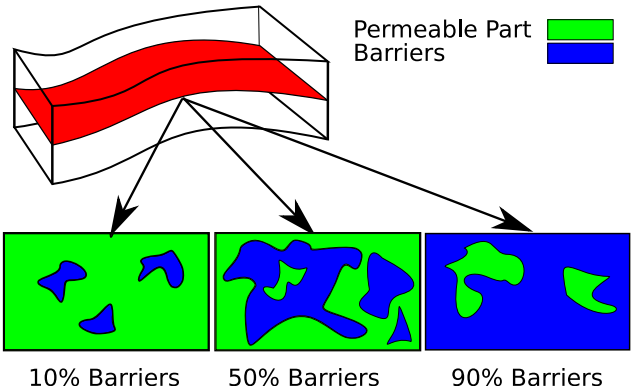

Figure 1.13: Periodic floods and flactuations in fluvial system can result in shale draped surfaces. These surfaces act as barriers to flow in both vertical and horizontal directions. The barries are modeled in the SAIGUP study by modifiying the transmissibility of cells across the barrier (red surface in the plot). Barrier level variations are specified by areal coverage of zero transmissibility multipliers (indicated by blue color).

supplied by the river compared to the accommodation space that the sea provides defines the transition of different rock-types between the river and the sea. If the river flux or sea level fluctuates, the equilibrium changes into a new bedding shape based on the balance of these factors.

When the river flux increases, it shifts the whole depositional system into the sea causing an angle between transitional deposits that are stacked on eachother because of this shifting. This angle is called aggradation angle. Three levels of aggradation are modeled here: low, medium and high (Fig. 1.14). As we will see later, aggradation can have a major role in influencing the CO_2 flow direction in the medium.

Progradation: Progradation is the depositional-dip direction between sea and river. Two types are considered here: up and down the dominant structural dip. Progradation combined with lobosity can influence the plume development in the medium, as the injected CO_2 plume migrates upward to the crest goes through heterogeneities (Fig. 1.15).

For more information about the geological modeling, see the special issue of the Petroleum Geosciences that is devoted to the SAIGUP study [48]. One selected realization of the SAIGUP models is

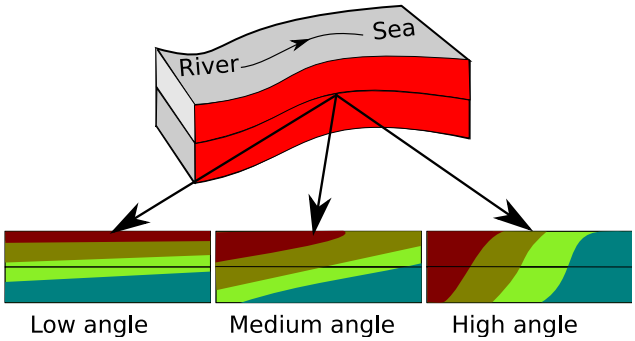

Figure 1.14: The change in the fluvial flux results in a shift in the depositional rock types from the river to the sea. The shift varies from very extensive in amount resulting in near horizontal layers of facies stocked on top of each other (low aggradation angles) to slight shifts resulting in near vertical rock type patterns (high aggradation angles).

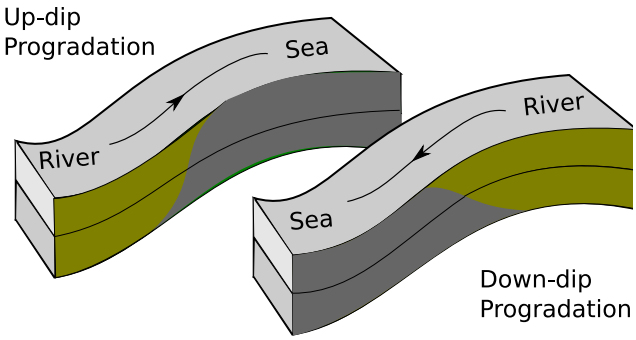

Figure 1.15: Techtonic activies in shallow marine systems can result in various orientations of river to sea depostions that is considered as progradation direction in the SAIGUP study.

available for download [65] and this model is used as an example in MATLAB Reservoir Simulation Toolbox (MRST) [66].

1.6 Flow equations

After introducing the parameters that make our geological model, we need to define the flow problem. In this section we discuss various formulations of the governing equations describing single and two phase flow in porous medium. Solution to this type of equations is implemented in the ECLIPSE black-oil simulator that we use to model the flow. We introduce the functionalities and axillary equations required to close the flow equation system. This section also includes a brief mathematical discussion on the flow equations. We discuss various flow regimes in the medium in the next section.

1.6.1 Single phase flow

Assume a porous domain Ω with boundary Γ as shown in Figure 1.16. We write the continuity equation in general form for a single phase flowing in the domain:

$$\text{Accumulation} + \text{In-Out Flux} = \text{Source/Sink} \tag{1.1}$$

$$\frac{d}{dt}\int_{\Omega}\phi\rho d\tau+\int_{\Gamma}\rho v\cdot nd\sigma=\int_{\Omega}qd\tau \tag{1.2}$$

In Equation 1.2, ϕ is the rock porosity, ρ is the fluid density, v is the Darcy flux, and n is the normal vector to the boundary. The term q denotes the mass source or sink in the system. Integrations are taken over arbitrary domain Ω with boundary Γ (Figure 1.16). Flow velocity is considered at the representative elementary volume (REV) scale for porous media [7].

The resistance of a porous medium against flow results in a flux that can be calculated from pressure and gravity gradient and fluid properties in the medium. This is governed by Darcy's law for incompressible single phase flow:

$$v=-\frac{K\rho g}{\mu}\cdot\nabla(\frac{P}{\rho g}+Z). \tag{1.3}$$

In Equation 1.3, K is the permeability of the medium. Z is the elevation in vertical direction and g is the gravitational acceleration. Here, we assume that the third coordinate axis aligns with the vertical direction; otherwise the equation should be modified to honor the gravitational acceleration vector projection on the coordinate axes (see [13]). Permeability is a function of pore size distribution and connectivity and in the macro scale, it is a measure of medium conductivity when a fluid is flowing through the medium (Figure 1.17). In general, density varies with pressure and Darcy equation takes the following form:

$$v=-\frac{K}{\mu}\cdot(\nabla P+\rho g\nabla Z). \tag{1.4}$$

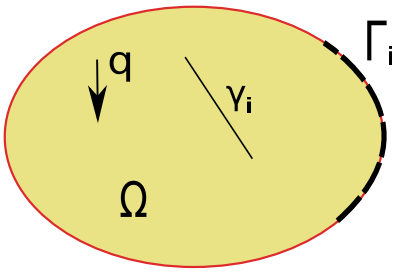

Figure 1.16: The flow problem is solved over domain Ω that is bounded by Γ_i. The injection well is modeled as source point q. Geological heterogeneities can be in the form of discontinuity γ_i.

Substituting v from Equation 1.4 into Equation 1.2 gives:

$$\frac{d}{dt}\int_{\Omega}\phi\rho d\tau-\int_{\Gamma}\rho\left(\frac{K}{\mu}\cdot(\nabla P+\rho g\nabla Z)\right)\cdot nd\sigma=\int_{\Omega}qd\tau. \tag{1.5}$$

As a primary unknown in Equation 1.5, the pressure depends upon the boundary conditions (as the second term in the left hand side of Equation 1.5 is an integration over the boundaries of the domain). Also, any geological discontinuities in the medium (γ_i in Figure 1.16) appears in Equation 1.5 through the K tensor and can influence pressure behavior in the domain.

We assume that $(\phi\rho)$ satisfies the Leibniz integration rule conditions. Then, the derivative in the first term of Equation 1.2 can enter the integral. The second term in Equation 1.2 can be converted into an integration over domain Ω, using divergence theorem resulting in the following:

$$\int_{\Omega}[\frac{\partial}{\partial t}(\phi\rho)+\nabla\cdot(\rho v)]d\tau=\int_{\Omega}qd\tau. \tag{1.6}$$

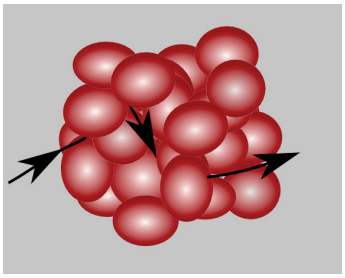

Figure 1.17: Permeability is an indication of how easy it is for the fluids to flow trough the medium.

Equation 1.6 is valid for arbitrary domain Ω, hence the equality is valid for the integrands *almost everywhere* in domain Ω in the *general* situation:

$$\frac{\partial}{\partial t}(\phi\rho)+\nabla\cdot(\rho v)=q. \tag{1.7}$$

Fluid and rock change in volume with pressure variations. These dependencies are defined by a parameter called total compressibility, which is approximated by a combination of rock and fluid compressibilities:

$$C_T \approx C_{rock}+C_{fluid}, \tag{1.8}$$

where

$$C_{rock}=\frac{\partial\phi}{\partial P}, \tag{1.9}$$

and

$$C_{fluid}=\frac{1}{\rho}\frac{\partial\rho}{\partial P}. \tag{1.10}$$

In Equation 1.9, C_{rock} can be assumed constant in moderate pressure changes depicting a linear relation between pressure and porosity. Assuming slight compression gives [62]:

$$\rho \simeq \rho_0+C_{fluid}\rho_0(P-P_0). \tag{1.11}$$

By substituting from Equations 1.8, 1.10, 1.9, and Equation 1.4 into Equation 1.7, assuming the spatial density variation to be zero (i.e., $\nabla\rho=0$), and by defining volumetric source/sink η, we have the single-phase diffusivity equation:

$$C_T\frac{\partial P}{\partial t}-\nabla\cdot[\frac{K}{\mu}(\nabla P+\rho g\nabla Z)]=\eta. \tag{1.12}$$

1.6.2 Two-phase flow

In a two-phase flow of CO_2 and water within porous media, interactions between phases lead to loss of energy. This introduces specific phenomena occurring in the pore scale that have impact on the macro scale flow performance. More complicated equations appear in modeling the two-phase flow compared to the single-phase problem. First, we describe some of the conceptual two-phase phenomena in the pore scale and then we will continue by deriving the flow equations for two phases in the system, i.e., CO_2 and water.

When CO_2 and water get in contact at the pore scale, an interface forms between them such that the energy in the system is minimized. Water and CO_2 are also in contact with the porous medium and the interface between them forms an angle from the solid phase in the water phase (shown by θ in Figure 1.18) that depends on their ability for wetting the rock. This is called wettability and the phase with

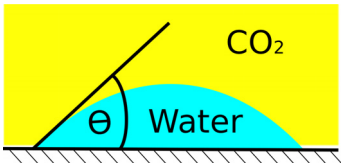

Figure 1.18: In a multiphase system, phases wet the medium with diffrent degrees of preference. Wettability is defined by the angle between two phases' interface and the solid surface (Θ). The wetting phase makes an acute angle with the solid phase. Water is the wetting phase in this example.

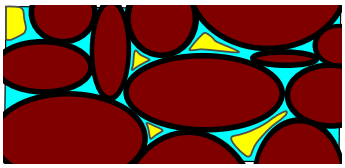

Figure 1.19: The CO_2 (yellow parts) is the non-wetting phase and it flows through the water (blue parts) that wets the rock grains (brown parts) easier than CO_2. The cross section of the medium is illustrated here.

the preference of wetting the solid phase is called the wetting phase. The other phase is called the non-wetting phase. Conventionally, θ is measured inside the denser fluid. If $\theta < \frac{\pi}{2}$ then the denser phase is the wetting phase. Wettability in a porous medium depends on the fluids and the rock. It can have a significant influence in the phase displacement within the medium. For water-CO_2 system, normally water is the wetting phase.

At very low water saturations, the water phase forms molecular films surrounding the rock grains. In this situation, the water phase is immobile and can not make a continuous phase moving through the porous medium. As water saturation in the medium increases, the layers covering the rock grains grow in size until the saturation exceeds the critical level, above which the water phase is able to flow in the medium. This saturation is called the critical or connate water saturation. In a water-wet rock, once the critical water saturation is reached (for example, during the first deposition of sediments), it can not go below that level by being displaced via a non-wetting phase. Therefore, when we inject CO_2 into an aquifer, there will always be some residual water saturation in the regions invaded by CO_2.

As a non-wetting phase, CO_2 flows in the middle part of the pore space as shown in Figure 1.19. If CO_2 saturation decreases in the medium, it reaches a critical level under which it can not make a continuous phase flowing through the pore-network. Tiny drops of CO_2 are trapped in the middle of the pore space and only very large pressure difference across the pore can move them out of the pore. This level of CO_2 saturation is called the residual saturation. Higher residual saturation is more interesting for the purpose of immobilizing more volumes of injected CO_2 in the aquifer, which reduces the risk of CO_2 leaking through any breakings in the geological formation and channeling toward surface.

Relative ease for the phase to flow within the medium is described by the relative permeability parameter. Relative permeability is a function of wettability and phase saturation. High phase saturation indicates a higher space available for the phase to flow through that space. A sample of CO_2-water relative permeability functions are shown in Figure 1.20. A library of relative permeability curves for CO_2-water system for various rock-types is available at [8].

The difference in surface tension between water and CO_2 causes a pressure acting on the interface of the two fluids. This pressure is called capillary pressure. In addition, capillary pressure depends on the geometry of pores. Since the pore geometry is very irregular, it is more convenient to use simpler geometry to derive the concept of capillary pressure. Therefore, experimental work in the laboratory is

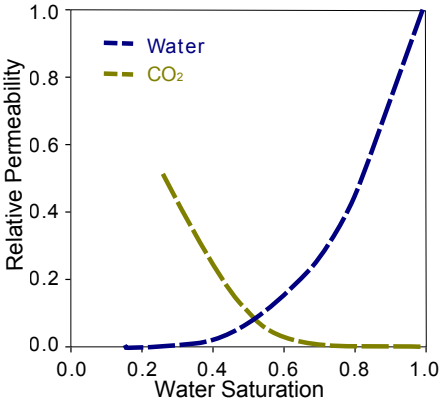

Figure 1.20: Relative permeability is an indication of how easy it is for the two phases to flow together through the medium. Relative permeability depends on the wettability of phases and the reltive volumes occupied by each phase (phase saturation).

required to specify the capillary pressure functionality in a special case.

Assuming a geometry of pipe to represent a pore structure, after balancing the forces in the pore-system capillary pressure can be written in the following form:

$$P_c = \frac{2\sigma}{r} cos\theta, \tag{1.13}$$

where σ is the interfacial tension, θ is the angle between the interface and the solid phase, and r is the radius of the pore.

Capillary pressure is a jump in phase pressure across the interface of the two phases. Therefore, we can relate it to the phase pressures:

$$P_c = P_{nw} - P_w. \tag{1.14}$$

Here, P_{nw} is the non-wetting phase pressure and P_w is the wetting phase pressure.

Capillary pressure can be expressed in an empirical relation as a function of wetting phase saturation. Lower capillary pressure is expected for higher wetting saturation, and capillary pressure value goes up for lower wetting saturation (Figure 1.21).

Assume hydrostatic equilibrium for a porous domain in which water and CO_2 are segregated due to buoyancy effect. If capillary forces are considerable in the domain, the sharp interface between water and CO_2 in the macro scale will be replaced by a transition zone with a spectrum of saturations between phases (Figure 1.23). Due to the hydrostatic equilibrium, phase pressure at each depth can be related to the hydrostatic pressure of that phase:

$$P_w = \rho_w g z, \tag{1.15}$$

$$P_{\mathrm{co}_2} = \rho_{\mathrm{co}_2} g z. \tag{1.16}$$

Having the phase pressure, capillary pressure can be calculated by Equation 1.14. As capillary pressure is a function of wetting saturation, the phase saturations can be back-calculated from this functionality and the phase saturation distribution over the medium can be found (Figure 1.22):

$$S_w = P_c^{-1}(S_w). \tag{1.17}$$

We can derive mass and momentum balance for two-phase flow, similar to what we have seen for single-phase flow. The equations must be written for each phase. In Equation 1.5, the accumulation term must be considered only for one phase mass calculated by multiplying the total accumulation mass

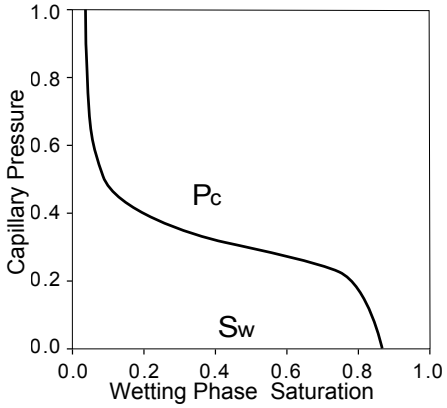

Figure 1.21: Capillary pressure can be expressed as a function of wetting saturation. The plot shows a typical Van Genuchten curve for capillary pressure. The scale in the vertical axis is only for demonstration. For application, see for example [46] and [40].

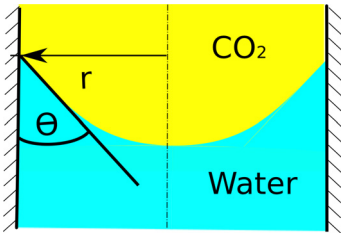

Figure 1.22: Capillary force is caused by the interaction of fluid phases with the pore walls. Capillary pressure is calculated from the force balance at the interface and depends on the curvature of the interface and the pore radius.

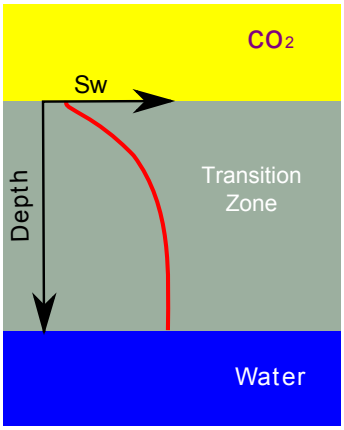

Figure 1.23: Water saturation (S_w) distribution in the capillary transition zone. In the hydrostatic equilibrium condition, phases exist at different depths with saturations that depend on the balance between capillary and gravity forces.

by phase saturation (S_α). Also the flux is the phase flux v_α, and the source/sink term must be written for the phase mass rate q_α.

For phase $\alpha = \{w \text{ for water}, CO_2\}$, we have:

$$\frac{d}{dt}\int_\Omega \phi \rho_\alpha S_\alpha d\tau + \int_\Gamma \rho_\alpha v_\alpha \cdot n d\sigma = \int_\Omega q d\tau. \tag{1.18}$$

Darcy equation for two phases $\alpha = \{w \text{ for water}, CO_2\}$ can be written in the following form:

$$v_\alpha = -\frac{K_{e\alpha}}{\mu_\alpha} \cdot (\nabla P_\alpha + \rho_\alpha g \nabla Z). \tag{1.19}$$

Here, $K_{e\alpha}$ is the effective permeability for phase α and can be calculated from:

$$K_{e\alpha} = K_{abs} K_{r\alpha}, \tag{1.20}$$

where K_{abs} is the absolute rock permeability and $K_{r\alpha}$ is the relative permeability of phase α. P_α is the phase pressure, ρ_α is the phase density, g is the gravitational acceleration, and Z is the elevation.

Similar to Equation 1.7, differential form of mass balance equation for each of phases $\alpha = \{w \text{ for water}, CO_2\}$ is as follows:

$$\frac{\partial}{\partial t}(\phi \rho_\alpha S_\alpha) + \nabla \cdot (\rho_\alpha v_\alpha) = q_\alpha. \tag{1.21}$$

In this equation, q_α is the source/sink mass rate for phase α.

The phase saturations are related by the following equation:

$$S_w + S_{co_2} = 1. \tag{1.22}$$

Fluid properties change by pressure and temperature. Density is mainly a function of pressure and viscosity depends upon temperature. These functions, called by convention equation of state (EOS), must be coupled to the system to honor fluid attribute variability [18, 31].

Mass exchange between phases may happen leading to change in composition. That also influences the fluid properties. In the immiscible fluids, the mass exchange can be in small order leading to slight changes in fluid properties. That can be modeled as a linear function with respect to pressure and temperature.

Extensive mass exchange between phases results in more nonlinear fluid property variations that require a detailed equation of state. Also for highly miscible fluids and high mass transfer between phases, it is better to write mass and momentum balance equations for components within phases in addition to phase equations.

There are a number of approaches to formulate the primary unknowns in the system of flow equations. The direct way is to replace phase velocities from Equation 1.19 into Equation 1.21, leaving the phase pressures and water saturation as the primary unknowns. This ends in a set of strongly coupled equations.

A popular approach for formulating the set of flow equations is the fractional flow method [10]. In this method the total multiphase flow problem is treated as a single-phase flux of multiphase mixture. Therefore, individual phases are described as a function of total flow. This leads to separate equations for pressure and saturation.

Pressure is defined for the total flow either globally or pseudo-globally and relates to the phase pressure and saturation with auxiliary equations. The fractional flow approach keeps the governing equations in the form of single flow equations, and numerical schemes for single-phase flow can be revised into efficient schemes for multiphase problems.

Pressure and saturation equations have different mathematical nature: pressure has a diffusive character of an elliptical nature, which is numerically more stable than the saturation equation. Saturation equation is of convection-diffusion form with hyperbolic character in the convection part. The convection operator in saturation equation can be highly non-linear due to strong coupling of saturation and phase flux. This nonlinearity can lead to shocks and discontinuities in the saturation solution.

As an example of fractional flow formulation, global pressure P_t is defined based on phase pressures:

$$P_t = \frac{1}{2}(P_W + P_{CO2}) - \int_{S_w|_{P_c=0}}^{Sw} (f_w - \frac{1}{2}) P'_c(S_w) dS_w, \tag{1.23}$$

where water fractional flow f_w is defined as:

$$f_w(S_w) = \frac{\frac{K_{rw}}{\mu_w}}{\frac{K_{rw}}{\mu_w} + \frac{K_{rco_2}}{\mu_{co_2}}}. \tag{1.24}$$

The total flux is defined as:

$$v_t = v_w + v_{co_2}. \tag{1.25}$$

If capillary and gravity effects are negligible, saturation equation can be solved analytically, e.g. via Buckley-Leverett technique, or method of characteristics.

1.7 Flow regimes

A major part of our studies includes modeling physical phenomena occurring within flow through porous media. Various phenomena occurs during a complete sequence of CO_2 sequestration. During injection, the forces imposed by the injector dominate the flow behavior in the region around the injector. When CO_2 plumes develop in a thin layer moving along the stratigraphical structure, the large interface between water and CO_2 enhances the diffusion phenomena and lets more CO_2 be dissolved into water. Convection of water with dissolved CO_2 leads to complicated flow regimes.

The injected CO_2 undergoes various stages until it is stored underground. We consider two stages in our studies: injection and early migration. Many forces act on flow within medium, each of which requires a set of modeling parameters. Simplifying assumptions for flow modeling can be justified at each stage with relevance to dominating forces in the medium.

The following can be recognized as forces acting on the medium at the scale at which Darcy flux is defined:

- Forces due to pressure gradients, mostly imposed by injectors (and/or producing wells).

- Buoyancy due to density contrasts between flowing phases. Gravity acts in the vertical direction.
- Capillary forces due to inter-facial tensions.
- Hysteresis due to sequencing of imbibition and drainage during flow in the porous medium.
- Convection forces due to gradients of density within one phase.
- Diffusion due to concentration gradients of one component.
- Reaction due to chemical reactions between phases and rock.

Modeling all forces acting on a porous medium is not practical, and we need to look at each flow regime separately by neglecting some forces that have a minor role. Herein, we discuss the main forces during injection and within long term migration.

1.7.1 Injection and early migration

Injection of CO_2 in the underground happens by forcing CO_2 mass through an injector into the medium. This poses a pressure gradient around the injector causing flow within the near bore region. Some authors call the force due to pressure difference 'viscous force', since viscosity has an important role in transferring the stress due to pressure difference in the porous medium resulting in fluid mobility. We use the same term throughout this thesis.

Viscous and gravity forces are the two major forces acting on the region around the injector during injection. Depending on fluid properties and distance from injection point, force balance changes. Gravity causes rapid phase separation resulting in upward movement of CO_2. Gravity forces dominate two-phase regions far from the injector with lower viscous flow velocity compared to near well locations, where the flow velocity is high. At each position in the medium, a force balance results in a total force vector that may cause flow in a particular direction (Figure 1.24a).

Attempts in the literature on evaluating force interplay during a multiphase flow regime incorporating injection in the porous medium, employ sensitivity analysis on flow attributes such as flow velocity and pressure. There a number of publications that discusses reducing a complicated flow problem into a simplified problem by taking plausible assumptions [9, 15, 17, 24, 25, 54, 58, 71, 72]. Utilizing analytical solutions gives the flexibility of examining a wide range of parameter variations within the model, enjoying a fast evaluation of the corresponding flow behavior. Semi-analytical and numerical sensitivity analysis are also practiced in the literature to involve more physical modeling features in the flow performance evaluations[2, 3, 61].

The flow equations can be normalized to a dimensionless version that is used in many studies discussing the capillary and gravity influence on the flow. Herein, we give the method reported in [25]. If we assume incompressible flow (i.e., constant phase density) and medium (i.e., constant porosity) in a one-dimensional domain Ω without any source/sink, Equation 1.21 reduces to the following for the wetting phase:

$$\phi \frac{\partial s_w}{\partial t} + \frac{\partial v_w}{\partial x} = 0, \tag{1.26}$$

and Darcy equation for one dimension flow becomes:

$$v_w = -K \frac{k_{rw}}{\mu_w} (\frac{\partial P_w}{\partial x} + \rho_w g z). \tag{1.27}$$

Here, x is the spatial direction in domain Ω, z is the vertical elevation and g is the gravitational acceleration. The system is closed by Equations 1.22 and 1.14 . We can define the dimensionless variables as follows:

$$X^* = \frac{x}{L};\ T^* = \frac{t v_t}{L\phi};\ \text{ and } P_c^* = \frac{p_c}{\pi_c}, \tag{1.28}$$

where L is a length constant in the problem, v_t is the total flux, and π_c is a capillary pressure normalizing constant. For incompressible fluids and a constant total flow rate, the total flux v_t equals the summation of phase fluxes:

$$v_t = v_w + v_{nw}. \tag{1.29}$$

After reformulating Equation 1.26, fractional flow can be written in the following form:

$$f_w = G(S_w) + C(S_w)\frac{\partial S_w}{\partial X^*}, \tag{1.30}$$

where S_w is the normalized wetting phase saturation, G is the gravity contribution, and C is the capillary contribution to the flow. The gravity and capillary contributions, G and C, are expressed by quantities relative to the viscous force [33] and we have:

$$G(S_w) = F_w(1 - N_G k_{rnw}), \tag{1.31}$$

$$C(S_w) = N_C F_w k_{rnw}\frac{\partial P_c}{\partial S_w}, \tag{1.32}$$

wherein:

$$F_w = \frac{\lambda_w}{\lambda_w + \lambda_{nw}}, \tag{1.33}$$

$$N_C = \frac{K\pi_c}{\mu_{nw} L v_t}, \tag{1.34}$$

and

$$N_G = \frac{K(\rho_w - \rho_{nw})gz}{\mu_{nw} v_t}. \tag{1.35}$$

Here,

$$\lambda_w = \frac{k_{rw}}{\mu_w}, \tag{1.36}$$

and

$$\lambda_{nw} = \frac{k_{rnw}}{\mu_{nw}}. \tag{1.37}$$

Having these definitions, Equation 1.26 reshapes into:

$$\frac{\partial S_w}{\partial T^*} + \frac{dG(S_w)}{dS_w}\frac{\partial S_w}{\partial X^*} + \frac{\partial}{\partial X^*}\left(C(S_w)\frac{\partial S_w}{\partial X^*}\right) = 0. \tag{1.38}$$

Applying specific type of capillary pressure and relative permeability function may lead to simplified forms of Equation 1.38 with the possibility of having an analytical solution [72].

Some important conclusions in the literature [9, 17, 25, 61, 72] from sensitivity studies on capillary, gravity and viscous forces are summarized here and inferred for CO_2 injection application:

- Gravity and capillary pressure will only influence the flow speed significantly for slow displacement rates. Therefore, around the injection point where normally fluids are flowing with a relatively high speed, viscous forces are dominant.
- If capillary is of any significance, ignoring capillary forces in modeling the injection of CO_2 results in a pessimistic CO_2 sweep efficiency. Capillary helps in the spreading of CO_2 in the frontal CO_2-water interface.
- Less capillary forces in the porous medium allows more space for CO_2. This enhances the density segregation due to gravity forces.

The main focus in the series of work in this thesis has been to assess the flow influence by heterogeneity during injection time and early CO_2 migration. For CO_2 injection problems, one objective is to maximize the rate of injection and aligned with that we use relatively high injection rates in our studies. Therefore, we did not include capillarity forces for modeling the high displacement rates within heterogeneities, which can be justified by the results in the literature.

Table 1.2: Spatial scales for CO_2 storage. Ranges are extracted from [13].

Feature	Spatial scale
Capillary fringe	10cm–>10m
Plume radius	10km–>100km
Pressure perturbation	50km–>500km
Migration distance	50km–>500+km

Table 1.3: Temporal scales for CO_2 storage. Ranges are extracted from [13, 32].

Feature	Temporal scale
Density segregation	1 month–>5+ years
Capillary segregation	1 year–>50 years
Injection period	5 years–>50 years
Convective mixing	20 years–>1000 years
Plume migration	few hundred years–>1000 years
Mineral reaction	500 years–>100000 years

1.7.2 Long term migration

The injected CO_2 volume in the geological formation will travel below the sealing cap by buoyancy forces due to the density difference between water and CO_2. The mobile CO_2 is at risk of leaking through any imperfections in the sealing layers and abandoned wells. Molecular diffusion occurs at the interface of water and CO_2 and this mass transfer from the CO_2 plume into water increases the water density. Transition of CO_2 from mobile phase into water with dissolved CO_2 is helping the safe storage of CO_2: the heavier water with dissolved CO_2 has the tendency of moving downward. Time scale for this convective mixing is of the order of several hundreds years (Table 1.3). Yet, this is not the end and the dissolved CO_2 can react with the porous medium ending up in a solid phase and it can be stored permanently in a process called mineral trapping. This is an extremely slow process and it can take thousands of years [32].

Mixing of CO_2 and water in the long-term happens through phases with various time scales and physical phenomena. Diffusion of CO_2 in water continues and layer of water with dissolved CO_2 builds up below the CO_2 plume until it forms heavy parts convecting in the form of unstable fingers, as shown in Figure 1.24b.

The onset time for the convective mixing is important in terms of storage safety. This time depends on the Rayleigh number in the medium:

$$Ra = \frac{Kg\Delta\rho H}{D_c\phi\mu}. \tag{1.39}$$

Here, $\Delta\rho$ is the density difference between the water and CO_2 phases, H is the formation thickness, and D_c is the molecular diffusion coefficient of CO_2 into water phase. The higher density sitting on top of lower density makes an unstable system and the medium must have a minimum Rayleigh number to have a growing instability for a small perturbation in the medium. Heterogeneities in the medium can initiate perturbations, reducing the instability onset time [20, 34]. Therefore, heterogeneity is an important factor that must be considered when we are choosing an aquifer for CO_2 storage.

Capillary fringe in the plume can enhance the onset of the convective mixing. It can speed up the process up to five times [22].

The flow equations for convective mixing are a set of mass and momentum balances for component $c = \{\text{Water}, CO_2\}$ within phase $\alpha = \{\text{Wetting}, \text{Non-Wetting}\}$:

$$\frac{\partial}{\partial t}\sum_{\alpha}\phi S_\alpha \rho_\alpha X_\alpha^c + \nabla\cdot\sum_{\alpha}\rho_\alpha X_\alpha^c v_\alpha = 0, \tag{1.40}$$

and

$$v_\alpha = -\frac{k_{r_\alpha} K}{\mu_\alpha} [\nabla P_\alpha - \rho_\alpha g z] \tag{1.41}$$

where X_α^c is the mole fraction of component c in phase α and v_α is the flux of phase α [21].

1.8 Flow modeling

We use a standard porous media simulator [64] to solve the flow equations in the medium. The simulator is based on finite volume method and the following assumptions are made:

- Two compressible phases are considered in the medium: water and super critical CO_2.
- No mass exchange occurs between the two phases.
- No heat exchange is considered.

1.8.1 Numerical scheme

The simulator uses a standard two-point finite difference scheme to solve Equation 1.21 on a corner-point grid. The Darcy equation for two-phase flow can be expressed based on algebraic difference terms. The equation governing the flow into cell a from the neighboring cell b is as follows:

$$F_{ab\alpha} = T_{ab} M_{a\alpha} \Delta\psi_\alpha. \tag{1.42}$$

Here, T_{ab} is the transmissibility of the medium between the two cells. $M_{a\alpha}$ is the mobility of phase α that is taken upstream of the flow from cell a and $\Delta\psi_\alpha$ is the potential term difference between two cell centers.

Transmissibility for two neighboring cells (i.e., sharing a face area, see Figure 1.25) is calculated by harmonic average of transmissibilities from the center of each cell to the center of the common face between the two cells:

$$T_{ab} = (\frac{1}{T_a} + \frac{1}{T_b})^{-1}. \tag{1.43}$$

Each half transmissibility, for example T_a, is calculated by an inner product between the permeability of the cell K_a, the mutual area A_{ab} between cells, and the distance from cell center to the mutual face center d_a:

$$T_a = K_a \cdot d_a \cdot A_{ab}. \tag{1.44}$$

The mobility term in Equation 1.42 is defined as follows:

$$M_{a\alpha} = \frac{k_{r\alpha}}{B_\alpha \mu_\alpha}, \tag{1.45}$$

where $k_{r\alpha}$ is the relative permeability of phase α, μ_α is the viscosity of phase α, and B_α is the formation volume factor of phase α, which is defined as :

$$B_\alpha = \frac{\text{Volume at surface condition}}{\text{Volume at formation condition}} = \frac{V_{s\alpha}}{V_{r\alpha}}. \tag{1.46}$$

This definition is connected to compressibility of the fluid, i.e., to changes in volume at the surface and at the geological formation condition. It is defined in this way in the simulator to consider cases where a fluid, such as oil, loses its dissolved gas while being produced at surface pressure. Since we assume no mass exchange between phases in our study, here the formation volume factor works like

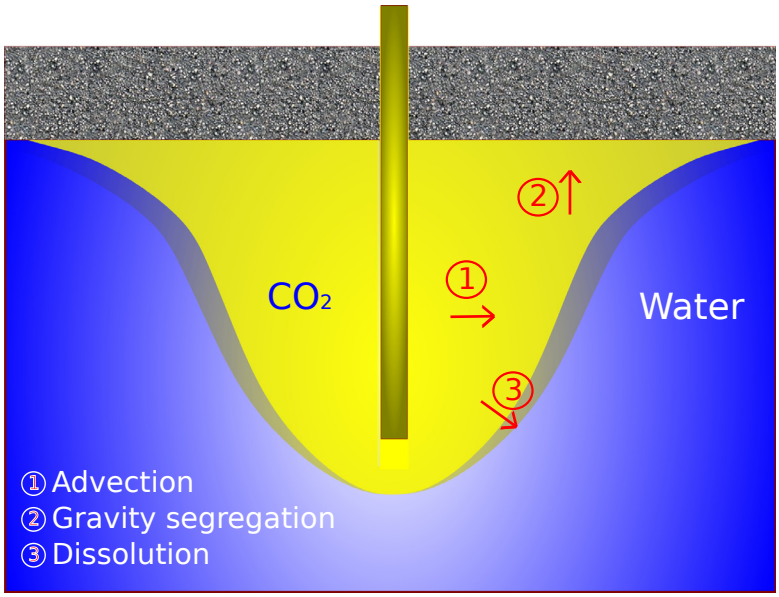

(a) Injection and early migration flow regime.

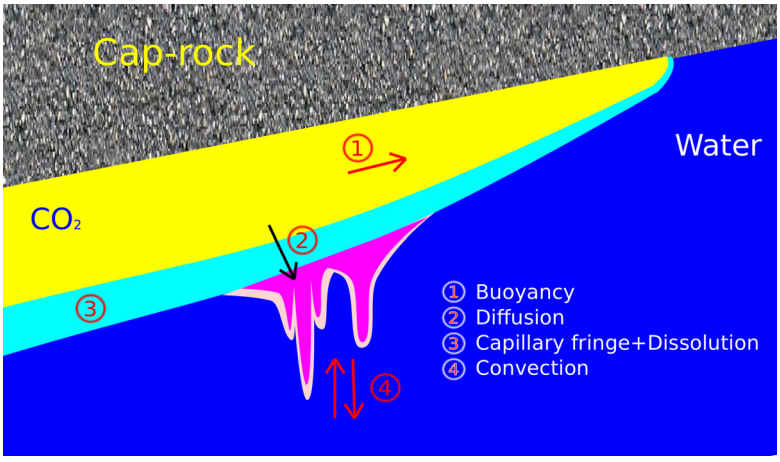

(b) Long-term migration flow regime.

Figure 1.24: Flow regimes in geological CO_2 storage; (a) During injection, the main physical processes are the flow advection due to the imposed pressure by the injection, the gravity segregation due to the phase density differences, and the dissolution of CO_2 into water. (b) During the long-term CO_2 migration, the main physical processes in the medium are the gravity segregation, the molecular diffusion, the CO_2 dissolution in water, the water capillary imibibition, and the convection mixing due to gravity instabilities.

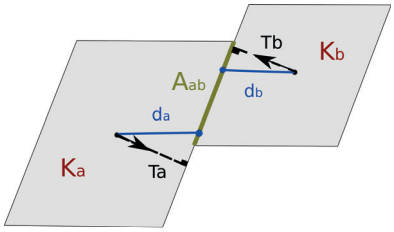

Figure 1.25: Transmissibility between two cells a and b depends on the interface area perpendicular to the flow (A_{ab}) and transmissibilities between the center and the cell side within each cell (T_a and T_b).

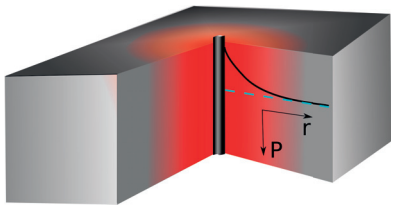

Figure 1.26: Injection operation causes pressure increase near the well-bore. The red color in the figure demonstrates the regions with pressure build-up. The well-bore pressure is calculated by a relation that models the pressure distribution around the well. The black curve in the figure shows a schematic incline of the pressure near the injector.

compressibility of the fluid. Formation volume factor is a function of pressure. Slight compressibility is considered for phases in our study, and phase density is defined as a function of pressure:

$$\rho_\alpha(P) = \frac{\rho_{0\alpha}}{B_\alpha(P)}. \tag{1.47}$$

Here, $\rho_{0\alpha}$ is the density of phase α at reference conditions.

Wells are defined as sources or sinks in Equation 1.21. In reality, wells are a void space drilled in the porous medium and the flow into the well-bore and up to the surface for production wells (and vice-versa for injectors) goes through a pressure change that must be modeled separately from the porous medium.

Figure 1.26 shows a schematic pressure distribution around the injector. The well radius is much smaller than the simulation cell containing the well and the pressure in the bottom-hole is different than the cell pressure. The well bottom-hole pressure can be related to the cell pressure containing the well by a separate approximation that can be coupled with flow equations in the grid model. Flow equation for phase α between the cell center and the well for an injector is written as follows:

$$\eta_\alpha = T_w \cdot M_\alpha \cdot [P_w - P_i]. \tag{1.48}$$

Here, η_α is the volumetric injection rate of phase α, P_w is the injector bottom-hole pressure, P_i is the cell pressure, T_w is the transmissibility between the cell and the injection well-bore, and M_α is the mobility of injection flow into the cell.

A region can be assumed by radius r_e at which the pressure is equal to the cell pressure. By approximating the flow near the well-bore using Equation 1.12, the transmissibility for this region can be found from the analytical solution of Equation 1.12:

$$T_w = \frac{K \cdot h}{ln(\frac{r_e}{r_w})}, \tag{1.49}$$

where h is the medium thickness, K is the medium rock permeability, and r_w is the well radius. Here, we assume that the well is completed and connected in the entire thickness h of the cell and there is no skin effect in the well. The Equation 1.49 can be extended to model wells with partial completions and skins. The effective radius r_e in Equation 1.49 is estimated from the Peaceman formula and can be related to the cell geometry:

$$r_e = 0.28 \frac{\left[\delta_x^2 (\frac{K_y}{K_x})^{\frac{1}{2}} + \delta_y^2 (\frac{K_x}{K_y})^{\frac{1}{2}}\right]^{\frac{1}{2}}}{(\frac{K_y}{K_x})^{\frac{1}{4}} + (\frac{K_x}{K_y})^{\frac{1}{4}}}. \tag{1.50}$$

Here, K_x and K_y are the permeabilities in x and y directions and δ_x and δ_y are the cell sizes in these directions. This equation assumes a vertical well and a diagonal permeability tensor. It can be modified for more general cases.

1.8.2 Flow scenarios

All of the SAIGUP realizations have dimensions of 3 km $\times$ 9 km $\times$ 80 m. The model spatial scales capture the typical geological features in a shallow-marine system, such as shore-line shape and aggradation angle variations. Various scales of heterogeneity can considerably impact the flow behavior. The lateral extent of the model is smaller than the scales used for CO_2 storage studies. In some storage sites, the lateral extent that the CO_2 travels can go to hundreds of kilometers. This makes our study limited in the spatial domain around the injector. For the same reason, in the temporal scale, we are more focused on injection and early migration time. We examine a number of injection scenarios to study the spatial distribution of CO_2 in the medium during injection and early migration periods.

The study of pressure is essential for injection operations. A detailed pressure study requires larger scales than what are used here. We choose open boundaries for the model to compensate for the actual large extents of a typical storage location (Figure 1.27). The choice of open boundary is not valid in domains that are bounded by structural seals. In fact, for the closed and semi-closed domains the pressure is a major control on the storage capacity along with other parameters. The results of our pressure study can change significantly by choosing different boundary conditions.

We model the boundary by large pore volumes on the outer closed cells. This makes the pressure to relax earlier than it does in a large domain. Even with such artifact, the effect of heterogeneities is clearly seen in a considerable fraction of cases with an extreme pressure build-up. We investigate the operational concerns related to pressure build-up for a typical injection scenario. Our pressure study can be used for devising mitigation plans by defining operational constraints for injectors. We perform an extensive probabilistic analysis on the CO_2 pressure behavior in the medium that can be applied in further studies with specific concerns about the pressure analysis.

We consider the injection of 20% of the total pore volume of the model(excluding the large volumes at the boundaries), which amounts to 40 MM m^3. This volume is injected into all realizations in three different scenarios. In the first scenario, the injection is forced to finish in 30 years and an unlimitted pressure rise in the system is permitted. Linear relative permeability functions are considered in this scenario. The purpose of the first scenario is to examine the flow distribution in the medium influenced by geological heterogeneity. Linear assumption for relative permeabilities is taken to speed up the flow within the medium. We have used quadratic relative permeability function in the second scenario. This scenario has shown a considerable increase in the pressure responses for many cases during CO_2 injection into the aquifer. This is mainly due to lower CO_2 mobility at low saturations compared to the linear relative permeability. Albeit, the CO_2 moving under a cap-rock will effectively have a linear relative permeability.

The third injection scenario is similar to the first scenario, except that the injector is controlled by pressure rather than volumetric rate. Thus, injection time is variable depending on the injectivity of the medium.

Only one injector is considered in the study. With one injector, it is easier to study the flow behavior and the plume development within the medium. The injector is located in the flank and to increase the

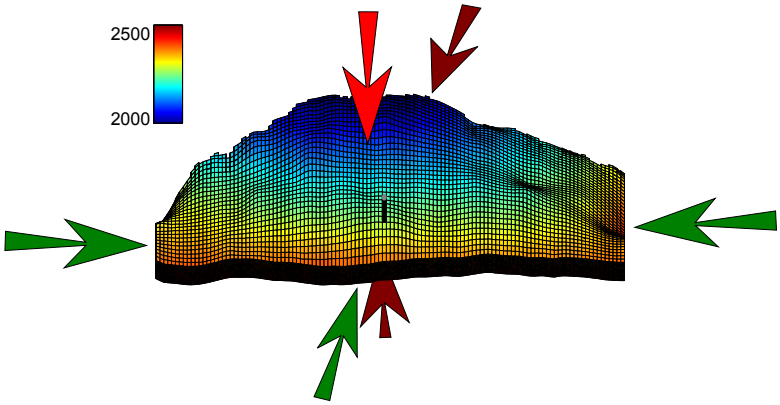

Figure 1.27: In the models used for flow simulation, the top, bottom, and upper side boundaries are closed and the rest are open to the flow. Arrows point to the boundaries and their color indicates if the boundary is open (green) or closed (red). Colors on the grid show the depth of different locations. The injector location is depicted by a black line.

sweep efficiency for the up-moving CO_2 plume, the injector is connected to the medium (completed) only in the lower part of the aquifer. The injector location and the completed layers are fixed for all of the realizations. The studies here aim to identify the influence of uncertainty on injectivity and fixing a place for injection helps in achieving this goal. As mentioned earlier, injectivity is a big player in the success of the operations. Uncertainty might be less near the well-bore region than in the larger scale in the domain, but requires costly operation data aquisition. Fixing the location of the well serves to specify the probability of having a feasible injectivity in different heterogeneities.

There are few locations of distorted geometries in the faulted realizations that may be considered as structural traps for the injected CO_2. The topography in the SAIGUP realizations is simple and does not cover the variational space to be used in a sensitivity analysis. The slight inclination in the structural geometry of the medium, from the flank up to the crest, leads the injected CO_2 to accumulate in the crest and below the faulted side of the aquifer. The structural trapping due to variational morphology is studied in IGEMS, which is a sister project to MatMora (for example, see [67]).

In a homogeneous medium, we expect the CO_2 to accumulate under the cap-rock. A small fraction of the injected CO_2 will escape through the open boundary near the injection well and the rest of it will stay within the medium in two forms that we refer to as mobile and residual volumes. As the CO_2 moves through the rock, part of it stays in the smaller pores due to the capillary trapping process and cannot be discharged by brine. The other parts move through the larger pores and can be displaced by water in an imbibition process. This volume is called mobile. As we are interested in storing the CO_2 permanently and safely, increasing the trapped volume is in line with the objective of minimizing the leakage risk and maximizing the storage capacity. Likewise, the more mobile volume of CO_2 exists in the medium, the higher will be the risk of leakage.

Defining the boundary conditions of the aquifer of interest can influence flow behavior in the system. Computational costs make it more feasible to model the flow locally and in the part of the aquifer that is going through more pronounced changes in flow behavior. Therefore, we can choose the boundaries of the model inside the aquifer in a volume that is containing the injection wells and the areas affected by them. Hydrostatic open boundary condition is a choice for the system boundaries to include the aquifer parts that fall outside the boundaries (Fig. 1.28).

The underground network of aquifer systems can be connected via geological channeling and conductive features. Some aquifers might be active and connected to the surface and expand in volume by variations in water influx due to seasonal rains. This can impose an external force on the system bound-

aries considered in the storage problems. Fig. 1.28 shows the water influx through the boundaries of the system due to external aquifer activities. We consider the external support by imposing a higher pressure than the hydrostatic pressure on the boundary of the model.

1.8.3 Flow responses

The primary unknowns in the flow model are the CO_2 pressure and the saturation distribution at different times. From the simulation output, we can derive quantities that address the feasibility of CO_2 injection. These quantities include a number of flow responses related to the CO_2 injection and migration problems. Each of these responses are directly or indirectly a measure of success for the operation within a specific realization. In the following, we give a brief description of each of them:

Total mobile and residual CO_2 volume: If the CO_2 saturation is below the critical value, it will be immobile in the bulk flow, although not in the molecular sense. Less mobile CO_2 means less risk of leakage. A more efficient volume sweep of CO_2 plumes can result in larger residual volumes (with saturations less than the critical). We use critical saturation value of 0.2 for both water and CO_2. During injection time the flow process is mainly drainage but after injection, imbibition also happens and increases the residual trapped CO_2.

Total number of CO_2 plumes and largest plume: To estimate the risk of leakage from the cap-rock, we assume that all mobile CO_2 connected to a leakage point will escape out of the reservoir. Hence, it is preferable if the total mobile CO_2 volume is split into smaller plumes rather than forming a big mobile plume. We looked at the largest plume size, the number of plumes, and other statistical parameters.

Average aquifer pressure: This is one of the most important responses to be considered. The pressure response in general shows a sharp jump at the start of injection and a declining trend during the injection and plume migration.

As soon as the injection starts, a pulse of pressure goes through the medium, introducing a pressure buildup in the aquifer. When the pressure wave reaches the open boundary, the aquifer pressure starts declining to a level maintained by the injector. When the injection operation stops, the pressure support will be removed and the pressure drops and declines until it reaches equilibrium.

Leakage risk: During injection operation the foremost important issue is the aquifer pressure, which as discussed earlier, may lead to fractures in the cap-rock. On the other hand, the cap-rock break depends on lithology and sealing thickness and differs from point to point. Some weaker locations can be the most probable to break and start leaking if any mobile CO_2 exists there.

An uncertainty assessment process consisting of geo-mechanical modeling of aquifer combined with flow modeling can cost a large amount of computations. To avoid expensive computations, the idea in this thesis is to model the possible breakings on the cap-rock (considering the stress stream in the medium) by introducing a probability measure on the cap-rock. This measure can be used to evaluate different cases for their risk of leakage, considering the CO_2 distribution under the cap-rock.

Here, we define the probability of leakage as a measure on the cap-rock that assigns a value to each point of the cap-rock, modeling the relative weakness of the cap-rock and the medium at that point. If for example both the cap-rock and the aquifer are continuous homogeneous layers with constant thickness, then the point of cap-rock that sits on the highest point of the injection slice can be the most probable place for leakage in the case of dramatic pressure increase in the well; the stress stream is more in the injection slice and the CO_2 accumulation occurs on the topmost part of the aforementioned slice. Then one may consider a 2D-Gaussian probability distribution on the cap-rock, centered above the injection slice.

If the medium is heterogeneous or tilted, the injected CO_2 may be distributed in different number and sizes of plumes below the cap-rock. Therefore, in addition to the probability of breaking for each point of cap-rock, one must consider the CO_2 connected volume that is attached to that point.

Since we have neither the cap-rock model nor the geo-mechanical properties of the SAIGUP models, we use a simple 2D-Gaussian leakage probability distribution centered at a point on the crest which is in the same slice as the injection point (Fig. 1.30). We calculate the probability of each cell in the

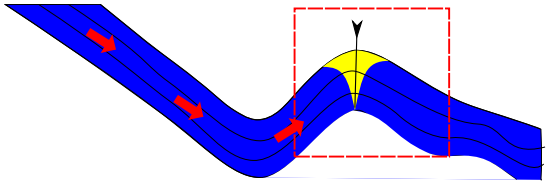

Figure 1.28: The aquifer can be connected to neighboring aquifer systems and the flow from those aquifers (red arrows in the plot) is modeled by imposing external pressure on the open sides of the model. The dotted box in the figure schematically indicates a domain considered for study. Aquifer layers outside the frame are considered external. The yellow color demonstrates the injected CO_2 in the aquifer.

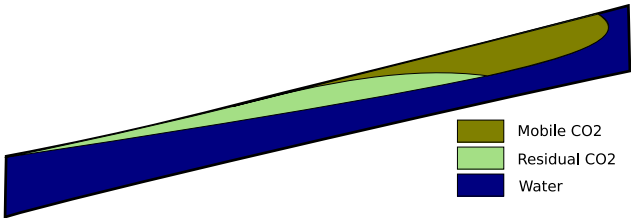

Figure 1.29: Mobile and residual CO_2 volumes; the injected CO_2 plume travels upward within the geological formation and leaves behind a volume of residual CO_2 that is trapped due to capillarity.

top layer and using the simulation results for the case, we weight it by the CO_2 saturation of that cell and the plume size that the cell is attached to. Summing up the values of the topmost cells, we assign a single number to the case, which we call leakage risk of the case. One may weight the case risk value with the average pressure in the system, such that higher pressure gives a bigger weight.

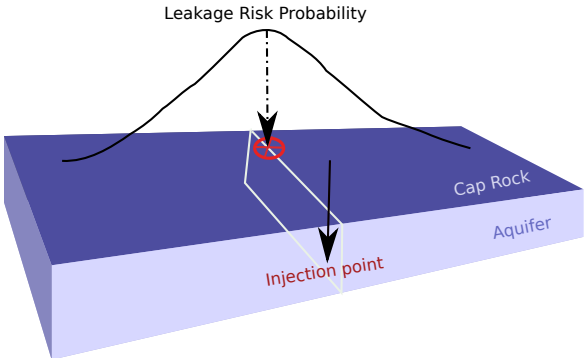

Figure 1.30: We use a 2D Gaussian distribution for leakage probability on the cap-rock.

Table 1.4: Geological heterogeneities for two selected cases.

Case	Fault	Lobosity	Barrier	Aggradation Angle	Progradation Direction
A	unfaulted	one lobe	50%	45°	down-dip
B	unfaulted	two lobe	50%	10°	up-dip

Results are discussed by comparing all cases in plots. However, the conclusions are made based on detailed flow study in some picked cases. For example, Figures 1.31 to 1.35 show the rock properties and CO_2 distribution in the domain at end of injection (i.e., after 30 years from the simulation start) and end of simulation (i.e., after 100 years from the simulation start) in two different cases. The heterogeneity description of the selected cases, called A and B, is given in Table 1.4.

CO_2 distribution in Figures 1.33 and 1.34 show that heterogeneity in case B has enhanced the lateral flow compared to case A. Direction of the flow can be seen in Figure 1.35. It is clear that heterogeneity can influence the imbibition and drainage process during and after injection. This, in turn, impacts the residual trapping process. The CO_2 plume can follow various paths through heterogeneities. In Figure 1.35a, the up-dip migration of CO_2 toward the crest pushes some volumes to move down-dip through high transmissibility channels.

Figure 1.36 demonstrates the plume evolution during simulation in two different cases, i.e., case A and B. The mobile CO_2 is plotted here and it shows that the injected CO_2 moves more in the vertical direction in case A, ending up in a big mass accumulated under the cap-rock. On the contrary, the heterogeneity in case B enhances the lateral movement of the plume, resulting in a laterally spread plume within the medium.

Figure 1.37 shows the development of pressure in the same cases. We see that injection in case B causes a dramatic pressure build-up due to the poor vertical transmissibility. The pressure build-up spreads out within the medium in case A, while it is trapped in the injection layers for case B.

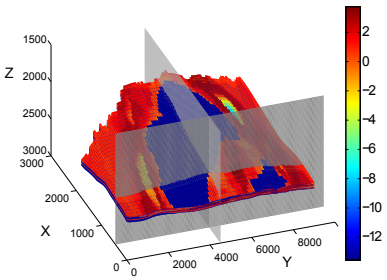

(a) Perspective view of model A

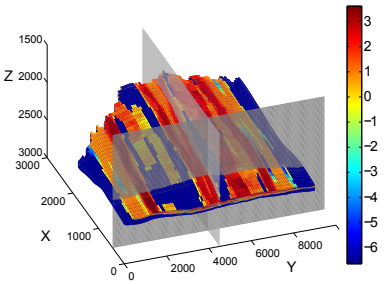

(b) Perspective view of model B

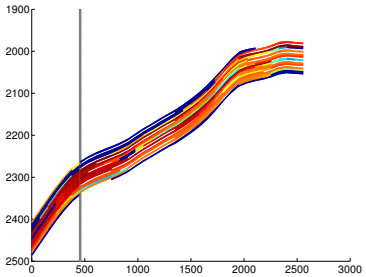

(c) The X slice at the injection point (see (a)).

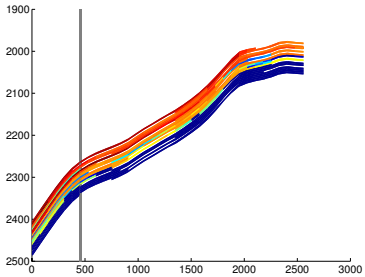

(d) The X slice at the injection point (see (b)).

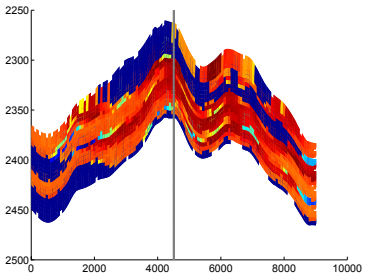

(e) The Y slice at the injection point (see (a)).

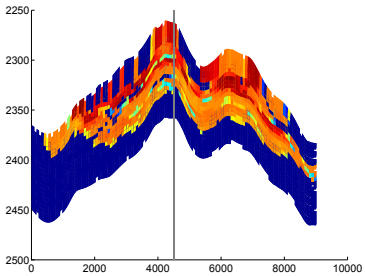

(f) The Y slice at the injection point (see (b)).

Figure 1.31: Transmissibility in the vertical direction for two selected cases. The left plots correspond to case A in Table 1.4, and the right plots belong to case B. Colors are in log scale and the scale in Figures (a) and (b) are powers of ten in cP.m^3/day/bar units.

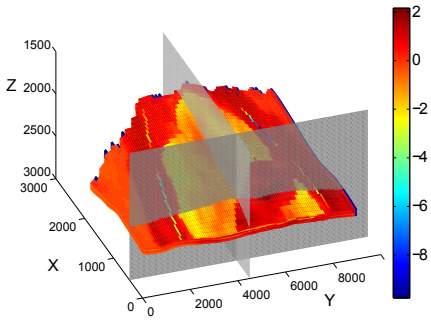

(a) Perspective view of model A

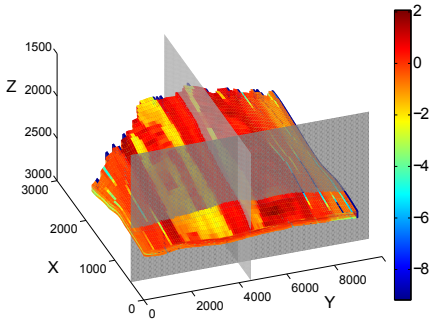

(b) Perspective view of model B

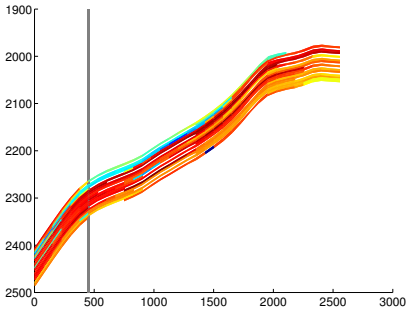

(c) The X slice at the injection point (see (a)).

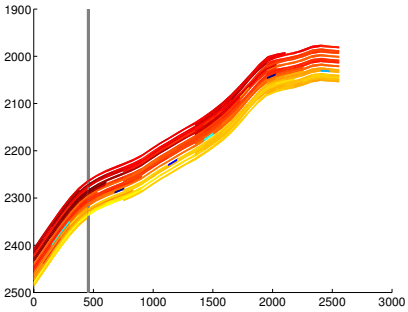

(d) The X slice at the injection point (see (b)).

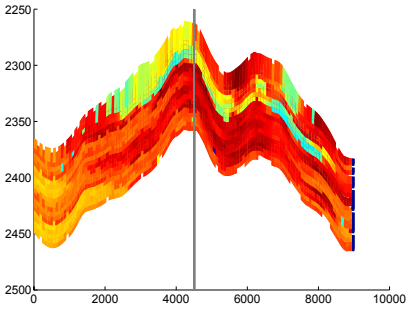

(e) The Y slice at the injection point (see (a)).

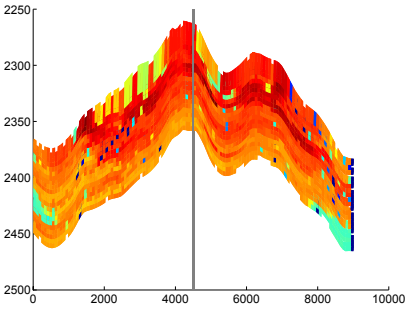

(f) The Y slice at the injection point (see (b)).

Figure 1.32: Transmissbility in the lateral direction for two selected cases. The left plots correspond to case A in Table 1.4, and the right plots belong to case B. Colors are in log scale and the scale in Figures (a) and (b) are powers of ten in cP.m^3/day/bar units.

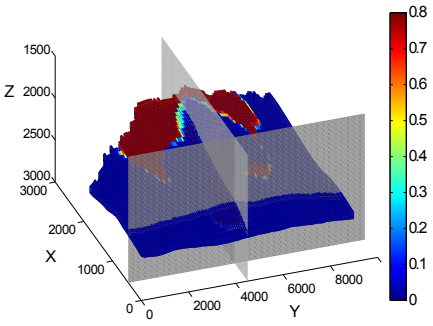

(a) Perspective view of model A

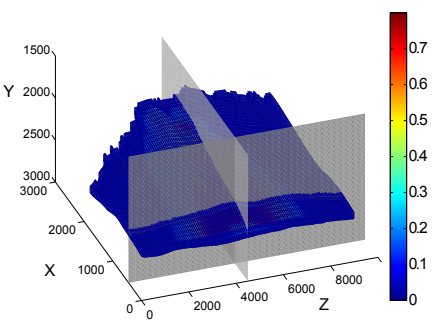

(b) Perspective view of model B

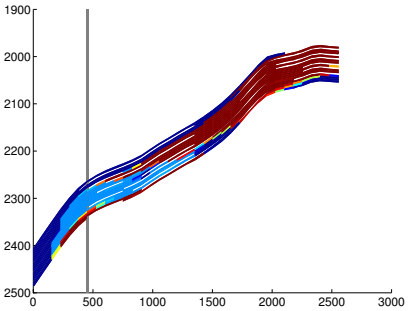

(c) The X slice at the injection point (see (a)).

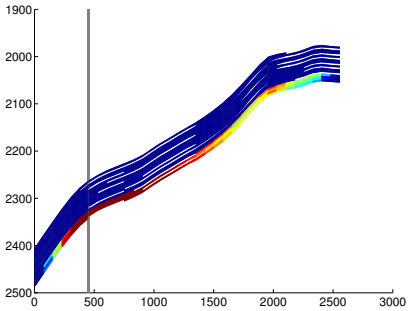

(d) The X slice at the injection point (see (b)).

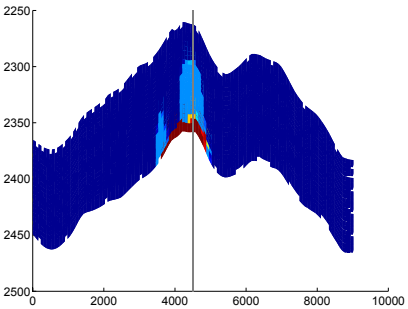

(e) The Y slice at the injection point (see (a)).

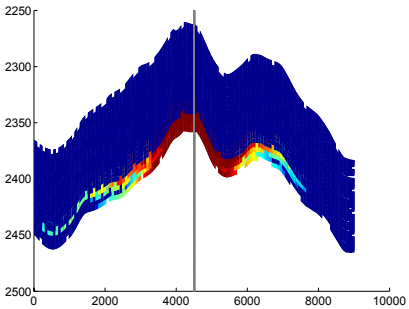

(f) The Y slice at the injection point (see (b)).

Figure 1.33: CO_2 distribution at the end of injection for two selected cases. The left plots correspond to case A in Table 1.4, and the right plots belong to case B.

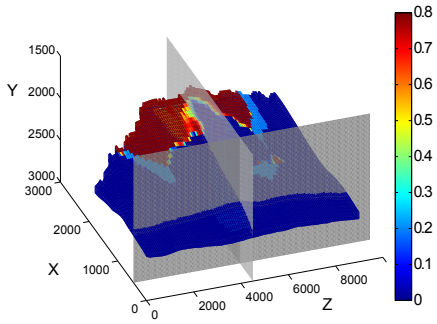

(a) Perspective view of model A

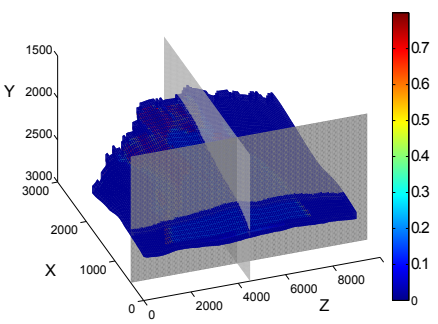

(b) Perspective view of model B

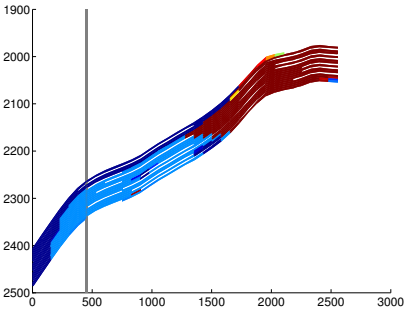

(c) The X slice at the injection point (see (a)).

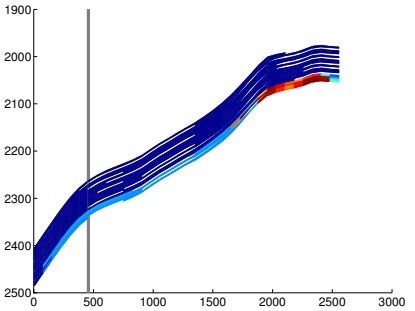

(d) The X slice at the injection point (see (b)).

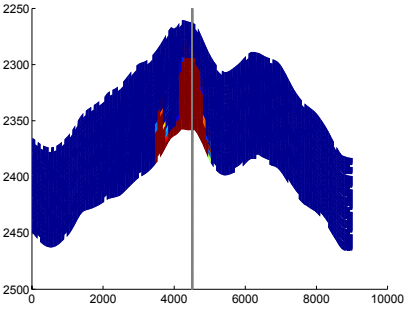

(e) The Y slice at the injection point (see (a)).

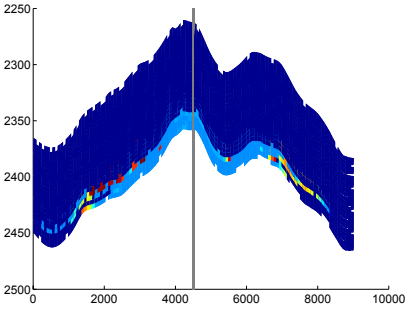

(f) The Y slice at the injection point (see (b)).

Figure 1.34: CO_2 distribution at the end of simulation for two selected cases. The left plots correspond to case A in Table 1.4, and the right plots belong to case B.

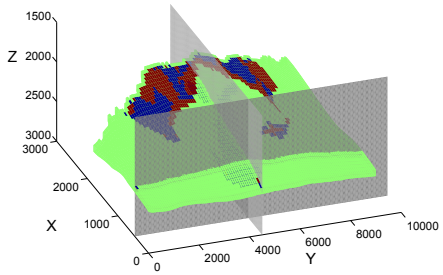

(a) Perspective view of model A

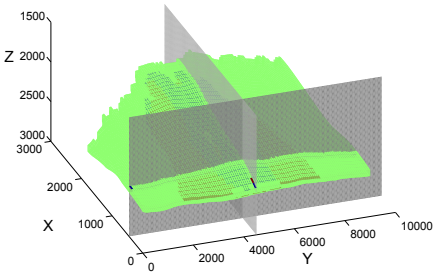

(b) Perspective view of model B

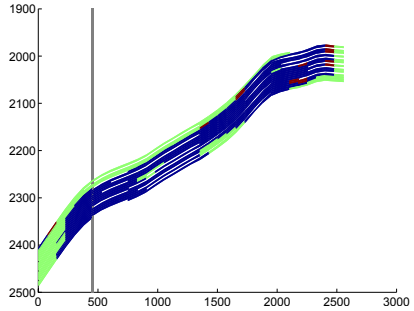

(c) The X slice at the injection point (see (a)).

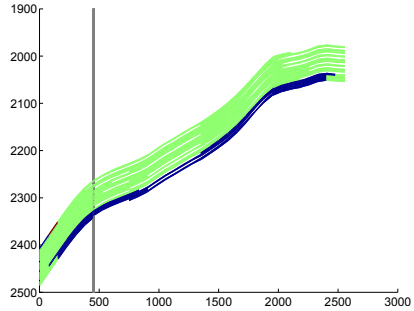

(d) The X slice at the injection point (see (b)).

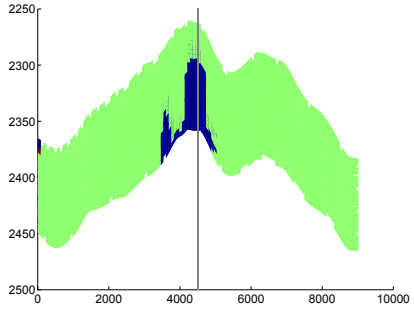

(e) The Y slice at the injection point (see (a)).

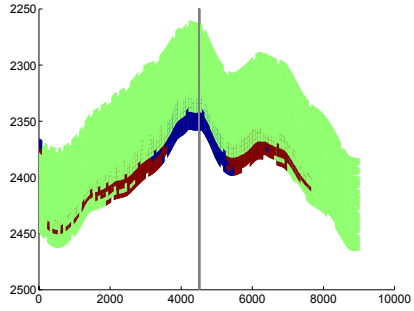

(f) The Y slice at the injection point (see (b)).

Figure 1.35: Flow sign in the X direction at the end of injection for two selected cases. The left plots correspond to case A in Table 1.4, and the right plots belong to case B. Red color corresponds to down-dip direction, blue to up-dip direction, and green represents the stagnant fluid.

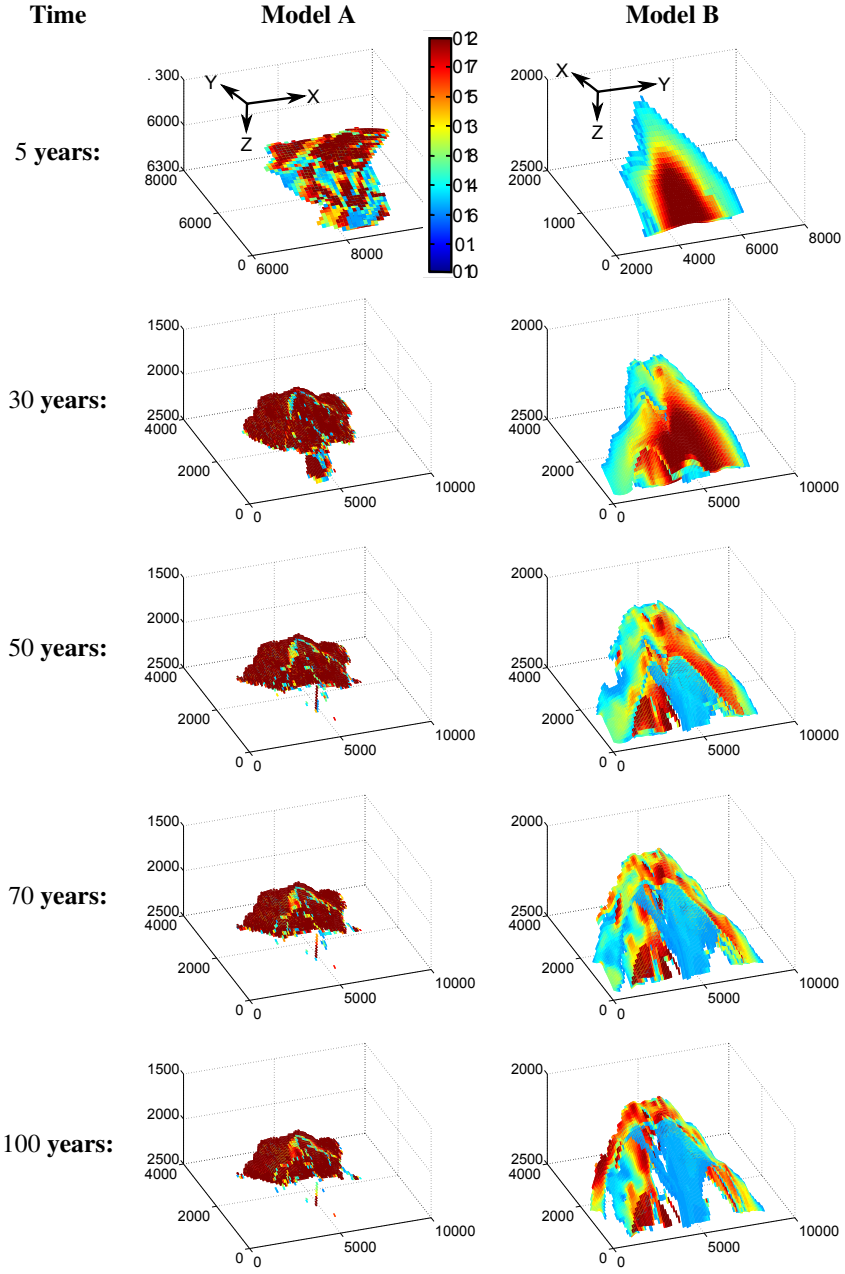

Figure 1.36: Mobile CO_2 distribution at different times for two selected cases. Cases A and B are described in Table 1.4. Compare with Figures 1.31 and 1.32 for transmissibility values in different directions. Colors represent the same ranges shown in the colorbar.

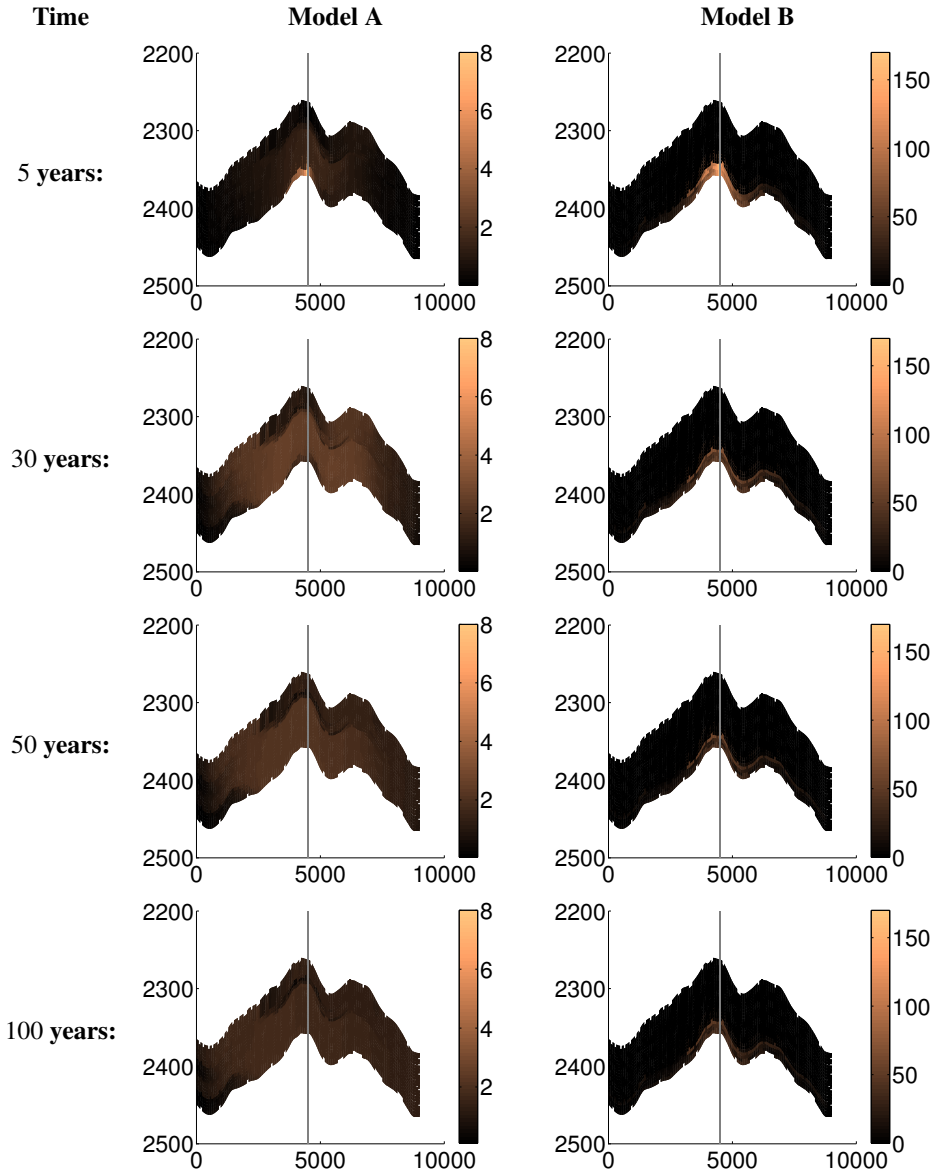

Figure 1.37: Pressure development during injection and early migration. Pressure differences from hydrostatic pressure are shown for two selected cases. Values are in bar. Cases A and B are described in Table 1.4. Compare with Figures 1.31 and 1.32 for transmissibility values in different directions.

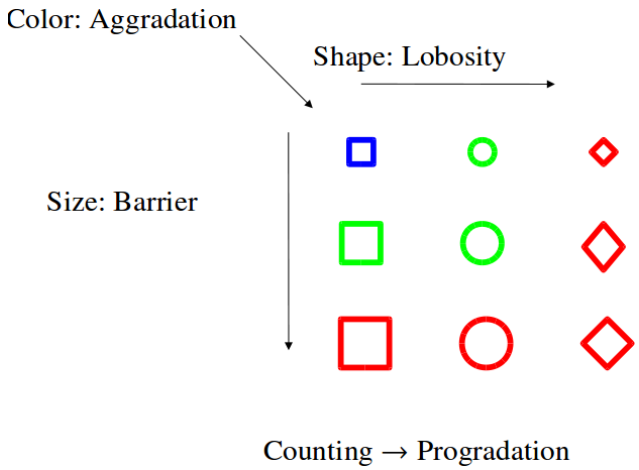

Figure 1.38: Marker codes used to plot the simulation results of all cases together. Aggradation is shown by different colors. Faults are shown by marker thickness; the thickest marker shows a case with close fault, medium thickness represents a case with open faults, and the thin markers indicate a case with no faults. All cases plotted in triples for the three degrees of faults. Therefor, plots contain 54 number of cases in the x-axis. The first 27 case numbers represent the up-dip progradation, and case numbers 28 to 54 have down-dip progradation.

One way to report the described responses and their relations to the uncertain parameters in one graph is to use scatter plots. Each case will then be represented by a marker sign with attributes dedicated to the set of geological parameter levels used in that case. Figure 1.38 shows some of the codes used in the study. This will be used later in the thesis and in the papers reporting our study.

1.8.4 ECLIPSE input file

In this section, important parts of the ECLIPSE input files that are used in modeling the flow are given. We will go through different sections of the ECLIPSE input file. It is assumed that the reader is familiar with the syntax and terminology used in the ECLIPSE simulation. See [64] for more information about ECLIPSE keywords. We use the version 2009 of ECLIPSE-100 black-oil module.

Several flow scenarios were examined before concluding in a few number of scenarios to be used in the study. Two main scenarios are considered that differ mainly in defining the well operational specifications. We will explain more about these cases in the SCHEDULE section. Only the important parts of the input file are given such that it is possible to reproduce the runs.

The model starts by specifying the general simulation settings: grid dimensions, phases involed in the study, simulation start date, and so on. We consider no mass exchange between water and CO_2. Therefore, it is enough to represent the flow by oil-water system where oil represents the CO_2 phase. We use CO_2 properties for oil:

```
RUNSPEC
DIMENS --Grid dimensions
40 120 20 /
--Two-phase flow problem with no mass exchange
WATER
OIL --CO2 is treated as OIL and CO2 properties used for it.
METRIC --Metric unit system
START --Simulation start date
1 'JAN' 2000 /
```

Then, the grid information are given for each realization. The set of keywords generated in the SAIGUP study are included in the input file. Each included file contains data for a specific keyword. Each file is named after the keyword name it includes with the extension 'INC'. For example, 'PORO.INC' contains the PORO keyword, which contains the porosity value for each cell in the model. Only two INCLUDE keywords are printed here to improve the readability of the code. In the second INCLUDE we provide the pore volume multipliers for the cells on the boundary of the model. This is used to represent hydrostatic open boundaries for three sides of the model.

```
GRID
INCLUDE -- Rock properties are included for each realization
'COORD.INC'/'ZCORN.INC'/'ACTNUM.INC'/'NTG.INC'/'PORO.INC'/
'PERMX.INC'/'PERMY.INC'/'PERMZ.INC'/
'MULTX.INC'/'MULTY.INC'/'MULTZ.INC'/
INCLUDE --Pore volume multipliers for the cells in the boundary
'MULTPV.INC'/ --1e6 and 1e3 values are used in different parts of the boundary.
```

In the EDIT section, we provide the fault transmissibility multipliers for each faulted case.

```
EDIT
INCLUDE
'EDITNNC.INC'/
```

In the PROPS section the relative permeability data are provided in two sets of tables with two different endpoints for CO_2 to consider the hysteresis effect. In the SOLUTION section, we use the first table to initialize the model with 100% water everywhere, and in the SCHEDULE section we use the second table to consider the residual CO_2 in a drainage process followed by an imibibition. In the presented scenario, linear relative permeabilities are used. Another scenario contains quadratic relative permeabilities that are given to the model similarly. Zero capillary pressure is used here. PVT data for CO_2 (modeled by OIL) and water phases, fluid viscosities, densities, and the rock-fluid compressibility models are provided here.

```
PROPS
SWFN
```

```
--   Sw      Krw      Pcow
     0.2     0.0       0
     1       1.0       0
/ --First table is used for time step zero
     0.2     0.0       0
     0.8     1.0       0
/ --Second table is used for the simulation
SOF2
--   So      Kro
     0.000  0.0000
     0.800  1.0000
/ --First table is used for time step zero
     0.200  0.0000
     0.800  1.0000
/ --Second table is used for the simulation

PVTW --Water PVT model
     200.0  1.0   3.03E-06   0.4   0.0 /
PVDO -- CO2 PVT model
     0.0     1.1   0.04
     400.0  0.95  0.04
/
ROCK --rock-fluid compressibility model
  400.0     0.30E-06 /
DENSITY --Phase densities
  700   1033     0.044/
```

In the REGIONS section we define different domains in the model. We specify the main domain that excludes the cells considered to represent the open boundaries. This is later used in the calculations of flow responses. Also, the saturation table is assigned here to be used in the initialization of the model as explained earlier.

```
 REGIONS
INCLUDE
'LRGNS.INC' /
SATNUM
96000*1/
```

The model is initialized here for the first time step by considering the hydrostatic equilibrium in the medium prior to CO_2 injection.

```
SOLUTION
--        DATUMz   Pi@DATUM    WOC      Pc@WOC   GOC   Pc@GOC
EQUIL
            2000          250      100         0      0      0       /
```

In the SUMMARY section we specify the output vectors to be used in our analysis.

```
SUMMARY
--   FIELD DATA
FPR
FOIP
FWIP
--   REGION DATA
ROIP
/
RWIP
/
RWSAT
/
RPR
/
--   WELL DATA
WBHP
/
WOIR
```

```
/
WVIR
/
```

Finally, in the main part of the model, we define the simulation scenario by providing the injector completion specifications and injection plan for the well. Here we see the SCHEDULE section that is considered for fixed injection rate over 30 years, followed by 70 years of early migration.

```
SCHEDULE
SATNUM --The second saturation table is assigned here to consider the hysteresis effects.
96000*2/
WELSPECS --Well drilling information
'I'  'G'   6  60  1*  'OIL'  /
/
COMPDAT --Well completion information
'I'  6   60     17  20 'OPEN'   0  .0   0.1/
/
WCONINJE --Well injection plan
'I' 'OIL' 'OPEN' 'RESV' 1*  3650.0 /
/
RPTRST
BASIC = 3 FREQ=1 FLOWS / -- FLOWS produces cell flux values for three directions.
TSTEP
0.1/
TSTEP
120*90 /
WCONINJE --Well is shut-in after 30 years
'I' 'OIL' 'SHUT' 'RESV' 1* 0.0 /
/
TSTEP
280*90 /
END
```

In the other scenario we control the well by pressure constraint and we continue the injection until the aimed total CO_2 volume is injected in the aquifer, or the simulation time reaches 100 years:

```
SCHEDULE
SATNUM --The second saturation table is assigned here to consider the hysteresis effects.
96000*2/
WELSPECS --Well drilling information
'I'  'G'   6  60  1*  'OIL'  /
/
COMPDAT --Well completion information
'I'   6   60     17  20 'OPEN'   3  .0   0.1/
/
WCONINJE --The injector is set to inject conditioned by a pressure lower than 400 bar
'I' 'OIL' 'OPEN' 'RESV' 1*  3650.0 400/
/
RPTRST
BASIC = 3 FREQ=8 FLOWS /
ACTION --Stop the well as soon as the total injected volume is 40000000 m3
STPINJ FOIT > 40000000 /
WCONINJE
'I' 'OIL' 'SHUT' 'RESV' 1* 0.0 /
/
ENDACTIO
TSTEP
0.1/
TSTEP --The simulation continues for a total 100 years
120*90 /
RPTRST
BASIC=3 FREQ=8/
TSTEP
280*90 /
END
```

We used a similar approach to the first scenario presented here with small modifications for the stochastic analysis that we will introduce in the next section.

1.9 Sensitivity and risk analysis

The process of developing mathematical models to approximate the injected CO_2 in the storage sites consist of several steps. This includes the determination of most influential parameters on the model outputs. Sensitivity analysis can serve as a guide to any further use of the model.

In the initial sensitivity analysis performed on geological uncertain parameters of our studies, we use a large number of detailed flow simulations and measure the variability of model responses with respect to each level of the uncertain parameters.

We can obtain histograms of response Γ for three different levels of parameter α (i.e., low, medium, and high) by performing simulations over all geological realizations. Measuring the mean response value on each histogram results in an average for all cases with a fixed level for parameter α. With three average points for low, medium, and high levels of parameter α, a line can be fitted to those points that approximates the trend of variations of response Γ versus the increase in values of parameter α.

With an equal probability for each level, the model output variations are examined by looking at each response at two important simulation times, i.e., end of injection and end of simulation. We need a fast flow modeler to assess the uncertainty with input variations over a relatively high resolution. We use a response surface method that is explained in the next section in details.

1.9.1 Stochastic analysis

Phenomenon for which variables are uncertain can be modeled as a stochastic process. Uncertainty reduction in different parts of the modeling requires a better understanding and description of input parameters and dependency rules within the system. Parameters can be ranked for their influence on the model output. To know the most influential parameters helps in treating the stochastic nature of the process. Sensitivity analysis serves in identification and evaluation of important model parameters.

As discussed in the earlier sections, various sources of uncertainties are embedded within CO_2 storage modeling and operations. The focus of our research has been on geological uncertainty and its consequences. The procedure used here to identify the relative importance of uncertain geological parameters via sensitivity analysis and the corresponding risk assessment is a general work-flow that can be applied to any type of uncertainties in the model inputs.

1.9.2 Arbitrary polynomial chaos expansion

Our research continues by employing stochastic response surface method that approximates the flow responses by projecting them on high-dimensional polynomials. In particular, we use arbitrary polynomial chaos (aPC) expansions, which consists of orthogonal polynomial basis that are constructed according to the uncertainties in the input parameters. The approach is flexible with respect to the quantification of probabilities for uncertain parameters and can be applied in studies with limited knowledge of probabilities.

The reduced model approximated by aPC is considerably faster than the original detailed one, thus provides a promising start point for global sensitivity analysis and probabilistic risk assessment. Variance-based global-sensitivity analysis methods have shown success in non-linear and complex problems [59]. The system can be decomposed into approximating functions of input parameters, and this makes it easy to implement methods based on variance. The bottleneck of variance-based approaches can be their computational costs. In our case, the variance in output responses can be set equal to the variance of polynomial components calculated for each input parameter. Polynomials are inexpensive to evaluate compared with full simulation. This makes it efficient to implement a variance based sensitivity analysis using polynomial approximation. Furthermore, the approach has been significantly

simplified by the fact that the polynomial properties of the response surface are known. The speed of polynomial approximation makes it feasible to perform an intensive probabilistic risk assessment via a Monte Carlo process over a high-resolution input variation.

Statistical accuracy of a Monte Carlo process is highly sensitive to the resolution of variational inputs. The response surface method assisting the Monte Carlo procedure must be constructed on a dense Cartesian grid, which will be computationally demanding. As a result, we explore an alternative method, which is a polynomial chaos expansion (PCE). This method only requires a minimum number of model evaluations to construct the approximating response surface. The approach we use is based on the aPC as described in [55]. The main idea is to construct the approximating response surface by projecting the response on orthogonal polynomial basis within the uncertain parameter space. Therefore, uncertainty in input parameters is involved in the process from the initial steps of the work-flow. This approach is an advanced statistical regression method that offers an efficient and accurate way of including nonlinear effects in stochastic analysis [23, 27, 73]. One attractive feature of PCE is the high-order approximation of error propagation as well as its computational speed [56] when compared to Monte Carlo processes.

Earlier PCE techniques put the restriction of specified types of uncertainty distribution functions to be used in the work-flow. In contrast, the arbitrary polynomial chaos (aPC) is flexible enough to accommodate a wide range of data distribution [55]. The aPC can even work in cases with limited uncertainty information reduced to a few statistical moments of samples. They can be specified either analytically as probability density, or cumulative distribution functions, numerically as histograms, or as raw data sets. In terms of performance, the aPC approach shows an improved convergence when applied to input distributions that fall outside the range of classical PCE.

In general, an approximation of system response Γ can be written as a function of uncertain input parameters Θ:

$$\Gamma \approx \Upsilon(\Theta). \tag{1.51}$$

Uncertainty of input parameters Θ can be represented by mapping h from random variable space ξ to random input space Θ

$$\Theta = h(\xi). \tag{1.52}$$

As discussed earlier, h can have an analytical or numerical representation.

The response of the system can be expanded into the space of approximating polynomial basis. This expression is specified by constant coefficients c_i:

$$\Gamma \approx \sum_{i=1}^{n_c} c_i \Pi_i(\Theta). \tag{1.53}$$

Here, n_c is the number of expansion terms, c_i are the expansion coefficients, and Π_i are the multi-dimensional polynomials for the variables $\Theta = [\theta_1, ..., \theta_n]$. The number n_c of unknown coefficients c_i depends on the degree d of the approximating polynomial, and the number of considered parameters n:

$$n_c = \frac{(d+n)!}{d! \times n!}. \tag{1.54}$$

For simplicity, we proceed with describing the procedure for one dimensional orthogonal basis. The high-dimensional basis can be obtained using tensor products on one-dimensional basis. Therefore, we consider the polynomial $P^{(k)}$ of degree k in the random variable θ:

$$P^{(k)}(\theta) = \sum_{j=0}^{k} p_j^{(k)} \theta^j. \tag{1.55}$$

where k can vary between 0 and d. Polynomials $P^{(k)}$ are orthogonal, if every pair of them fulfill the following condition:

$$\int_{I\in\Omega} P^{(l)}P^{(m)}d\tau(\theta) = \delta_{lm}, \tag{1.56}$$

where δ is the Kronecker delta function and τ is the measure for input variable space. If we modify the polynomials $P^{(k)}$ such that the coefficient of leading terms with the highest degree becomes one (i.e., $p_k^{(k)} = 1$), the orthogonal polynomial basis satisfying Equation (1.56) can be obtained from the solution of the following linear system of equations [55]:

$$\begin{bmatrix} \mu_0 & \mu_1 & \dots & \mu_k \\ \mu_1 & \mu_2 & \dots & \mu_{k+1} \\ \dots & \dots & \dots & \dots \\ \mu_{k-1} & \mu_k & \dots & \mu_{2k-1} \\ 0 & 0 & \dots & 1 \end{bmatrix} \begin{bmatrix} P_0^{(k)} \\ P_1^{(k)} \\ \dots \\ P_{k-1}^{(k)} \\ P_k^{(k)} \end{bmatrix} = \begin{bmatrix} 0 \\ 0 \\ \dots \\ 0 \\ 1 \end{bmatrix}. \tag{1.57}$$

Here, μ_k is the k^{th} non-central (raw) statistical moment of the random input variable, which is defined as:

$$\mu_k = \int_{\theta\in\Omega} \theta^k d\tau(\theta). \tag{1.58}$$

Thus, arbitrary polynomial chaos expansion based on Equation 1.57 only demands the existence of a finite number of moments, and does not require the exact knowledge or even existence of probability density functions. If the moments of θ are evaluated directly from a data set of limited size or from a discrete probability distribution featuring a finite number of possible outcomes, there need to be k or more distinct values in the data set or distribution. An interesting aspect is that only moments up to twice the order of the expansion are important. This means that there is no need for any kind of assumption for data probability distribution leading to subjectivity artifacts as discussed earlier.

The PCE techniques are divided into intrusive [30, 49, 70] and non-intrusive [41, 43, 44, 56] approaches. Intrusive techniques require modification of the system of governing equations (e.g., the flow model system). In some cases, this can end up in semi-analytical methods that are used for simpler stochastic analysis studies (e.g., stochastic Galerkin method). However, the intrusive approaches can be very complex and analytically cumbersome and cannot be implemented for industrial applications. In contrast to intrusive techniques, the non-intrusive methods are vastly used in practical studies. These methods do not require any symbolic manipulations of the governing equations. The sparse quadrature and the probabilistic collocation method (PCM, [44, 56]) are among the non-intrusive techniques. In a simple sense, PCM can be considered as a mathematically optimized interpolation of model output for various parameter sets. The polynomial interpolation is based on minimal model evaluations in an optimally chosen set of parameter locations that are called collocation points. Hence, the challenge in these techniques is to find a balance between accuracy and speed to evaluate the uncertainty in the physical processes.

The collocation formulation has the advantage of treating the model as a black-box. This formulation requires the corresponding output to be known in the collocation set of input parameters.

According to [69], the optimal choice of collocation points corresponds to the roots of the polynomial of one degree higher $(d+1)$ than the order used in the chaos expansion (d). This strategy is based on the theory of Gaussian integration (e.g., [1]).

For multi-parameter analysis, the full tensor grid of available points from the original integration rule is $(d+1)^n$, which is larger than the necessary number M of collocation points. This might be used for low-order (1^{st}, 2^{nd}) analysis of limited number of parameters. However, for a large number of parameters and high order of polynomial approximations, the full grid becomes computationally cumbersome. In the collocation approach, the minimal set of points is chosen from the most probable regions based on the parameter uncertainty information (See [44, 55, 56]).

We implement the probabilistic collocation method for computing the coefficients c_i in Equation 1.53. The weighted-residual method in the random space is defined as [44]:

$$\int \left[\Gamma - \sum_{i=1}^{n_c} c_i \Pi_i(\Theta)) w(\Theta) p(\Theta) \right] d\tau = 0, \tag{1.59}$$

where $w(\Theta)$ is the weighting function and $p(\Theta)$ is the joint probability density function of Θ. By substituting the weight function in Equation 1.59 with Delta function, the equation reduces to

$$\Gamma_c - \sum_{i=1}^{n_c} c_i \Pi_i(\Theta_c) = 0. \tag{1.60}$$

In this equation, Γ_c and Θ_c are the responses and input parameters in the collocation points. If we have Θ_c chosen based on the probability distribution of input parameters, and Γ_c from the minimal model evaluations on Θ_c, we can solve Equation 1.60 and find the coefficients c_i.

1.9.3 Sensitivity analysis

Sensitivity analysis helps in understanding the degree of dependency of system responses to input parameters. When the value of the input parameters is uncertain, the model prediction will consist of uncertainties that must be eliminated for a robust and precise prediction. Therefore, sensitivity analysis can be useful both in optimizing the system performance and in studying the variation in performance coming from the stochastic nature of the system.

Global sensitivity analysis covers the entire variational space for uncertain parameters, while other methods, like the gradient-based methods, are limited to the parameters' scope of influence.

Variance-based methods are very popular among different types of sensitivity analysis methods. Variance-based methods provide global sensitivity and are suitable for general non-linear problems. When the response is decomposed into simpler components (for instance, polynomial basis), it is easier to decompose the unconditional variance in the output into terms due to individual parameters and the interaction between them. It is possible then to rank the input parameters based on their contribution to the output variance [59, 63].

Following the linear sensitivity analysis initially performed in the study about the extensive detailed simulations, we tackle the global sensitivity analysis based on the aPC technique. This approach is well described in [55, 57]. Morris method [52] considers a uniform importance of input parameters within predefined intervals. We use a weighted global sensitivity in a more flexible approach accounting for arbitrary bounds and parameters with different importance defined by weighting functions. The big advantage of aPC-based sensitivity method is its low computational costs for obtaining global sensitivity analysis. The aPC based-method places the parameter sets for model evaluation at optimized spacing in parameter space. This can be interpreted as fitting polynomials to the model response. These polynomials approximate the model over the entire parameter space in weighted least-square sense. This is beneficial to compute tangent or local second derivatives (compare FORM, SORM methods, e.g., [42]) that approximate the model well just around one point in the parameter space.

As an advantage, in variance based methods one can work with arbitrary system as a black-box and perform the calculations based on inputs and outputs only. More recent works are concerned about expediting calculation pace [16, 55, 57]. The idea is to replace the system with an approximating function which gives benefits in sensitivity calculations, because it is easy to relate the output variances to the input variables.

We expand the variance of output solution into components. Assume that we break the system output into components:

$$\Gamma = \Gamma_0 + \sum_i \Gamma_i + \sum_i \sum_{j>i} \Gamma_{ij} + \ldots \tag{1.61}$$

A single index shows dependency to a specific input variable, whereas more than one index shows interaction of input variables. If we consider input vector Θ to be of n components θ_i for $i = 1, .., n$, then

$\Gamma_i = f_i(\theta_i)$ and $\Gamma_{ij} = f_{ij}(\theta_i, \theta_j)$. In practice, we consider a finite number of terms in Equation (1.61). The first order sensitivity index, so called Sobol index, is defined as follows [63]:

$$S_i = \frac{\mathrm{V}[\mathrm{E}(\Gamma \mid \theta_i)]}{\mathrm{V}(\Gamma)}, \tag{1.62}$$

where $\mathrm{E}(\Gamma \mid \theta_i)$ is the conditional expectation of output Γ given θ_i and V is the variance operator. Since θ_i can be fixed at any value in its uncertainty interval, each of those values produce a distinct expectation $\mathrm{E}(\Gamma \mid \theta_i)$. Equation 1.62 is a measure for variation of these expectations, which indicates the direct contribution of parameter θ_i in the output variance. For more than one index, a higher-order Sobol index can be defined as:

$$S_{ij} = \frac{\mathrm{V}[\mathrm{E}(\Gamma \mid \theta_i, \theta_j)] - \mathrm{V}[\,\mathrm{E}(\Gamma \mid \theta_i)] - \mathrm{V}[\mathrm{E}(\Gamma \mid \theta_j)]}{\mathrm{V}(\Gamma)}. \tag{1.63}$$

Here, $\mathrm{V}[\mathrm{E}(\Gamma \mid \theta_i, \theta_j)]$ is the variance of output expectations after fixing θ_i and θ_j. This index represents significance of variation in output generated from uncertainty in input variables together, i.e., the interaction of uncertain parameters. If we add all indices that contain variable θ_i, the sum is called the total Sobol index:

$$S_{Ti} = S_i + \sum_{j \neq i} S_{ij} + \sum_{j \neq i} \sum_{k \neq i} S_{ijk} + \ldots \tag{1.64}$$

To clarify the subject, we go through a simple analytical example given in [4]. Suppose that the exact expression for response Γ is known and can be written as a polynomial with parameters θ_1, θ_2, and θ_3:

$$\Gamma(\theta_1, \theta_2, \theta_3) = {\theta_1}^2 + {\theta_2}^4 + \theta_1\theta_2 + \theta_2{\theta_3}^4. \tag{1.65}$$

The Sobol indices can be calculated from functions F that are defined based on orthogonality condition used to decompose the solution and for n-dimensional input with Gaussian distribution Φ_n in uncertainty domain R^n. They are as follows:

$$F_0 = \int_{R^n} \Gamma(\Theta)\Phi_n(\Theta)d\Theta, \tag{1.66}$$

$$F_i = \frac{\int_{R^{n-1}} \Gamma_{|_{\theta_i}} \Phi_{n-1}(\theta_{\sim i})d\theta_{\sim i}}{\Phi_1(\theta_i)} - F_0, \tag{1.67}$$

$$F_{i,j} = \frac{\int_{R^{n-2}} \Gamma_{|_{\theta_i,\theta_j}} \Phi_{n-2}(\theta_{\sim i,\sim j})d\theta_{\sim i}d\theta_{\sim j}}{\Phi_2(\theta_i, \theta_j)} - F_0 - F_i(\theta_i) - F_j(\theta_j). \tag{1.68}$$

$\Gamma_{|_{\theta_i}}$ and $\Gamma_{|_{\theta_i,\theta_j}}$ are the Γ values at fixed θ_i and $\{\theta_i, \theta_j\}$ respectively. $\theta_{\sim i}$ is the vector of dummy variables corresponding to all but the component θ_i of uncertain parameters Θ.

Let us denote the variances by D:

$$D = \mathrm{V}[F(\Theta)] = \int_{R^n} F^2(\Theta)d\Theta - F_0^2, \tag{1.69}$$

that can be decomposed into:

$$D_i = \int_{R^1} {F_i}^2(\theta_i)d\theta_i, \tag{1.70}$$

and

$$D_{i,j} = \int_{R^2} {F_{ij}}^2(\theta_i, \theta_j)d\theta_i d\theta_j. \tag{1.71}$$

Then the Sobol indices can be found from:

$$S_i = \frac{D_i}{D}, \tag{1.72}$$

$$S_{i,j} = \frac{D_{i,j}}{D}. \tag{1.73}$$

Finally, the total Sobol index can be found from Equation 1.64. When we perform the calculations of Equations 1.66 to 1.71 for our example (i.e., the expression in Equation 1.65) we can obtain the following Sobol indices, assuming Gaussian distributions for the parameters over the interval $[0,1]$:

$S_1 = 0.0005 \quad S_2 = 0.4281 \quad S_3 = 0.0000$
$S_{12} = 0.0007 \quad S_{13} = 0.0000 \quad S_{23} = 0.5708$
$S_{123} = 0.0000$

and the total sobol indices are:

$S_{T1} = 0.0012 \quad S_{T2} = 0.9996 \quad S_{T3} = 0.5708$.

The total Sobol index can be used as a sensitivity measure to rank parameters for their influence on the results variation. In this example, we can see the ranking that the total Sobol indices suggests is consistent with what can be inferred directly from the simple expression in Equation 1.65: θ_2 is the most influential parameter, because it appears in three terms, and in one of them with a forth degree. Interactions are represented by two indices, and S_{13} is zero, because there exist no term in Equation 1.65 that contains both θ_1 and θ_3.

With known polynomial coefficients, Sobol indices are easy to calculate. When the number of parameters is large, it is possible to do initial sensitivity analysis with lower degree polynomial to filter out pertinent parameters. Then the analysis continues on the filtered parameters with a higher degree polynomial approximation.

1.9.4 Risk analysis

The risk is the impact of uncertainty on objectives. Quantifying the risk requires calculating this impact, which consist of two parts: quantification of the uncertainty and evaluation of the system consequences. Risk R of a process is quantitatively defined as the consequence C caused by the process multiplied by the probability P of that consequence to happen:

$$R = P \times C. \tag{1.74}$$

In the case of CO_2 injection into deep aquifers, the amount of CO_2 which stays mobile and undissolved in the medium for a time after injection can be considered as a consequence, bearing the potential of leakage up to the surface if exposed to a geological leakage point. The risk could be the expected amount of CO_2 that will leak through ill-plugged abandoned wells or cracks in the sealing rocks.

We consider looking at responses and the probability of them to happen. We initially examine this probability by drawing the histogram of response values obtained from detailed simulations on large number of realizations at end of injection and end of simulation. Yet larger number of points in the uncertain parameter space are studied employing the data-driven aPC method, which requires a considerably shorter time for evaluating the responses than what takes for a full simulation. This way it is possible to perform an intensive Monte Carlo process in a full tensor grid of input parameter variational space, resulting in a high resolution output probability distribution.

1.10 General summary

The work objectives were as follows:

- Assessing the significance of geological modeling in early stages of CO_2 storage operations.
- Applying a mathematical tool to perform global sensitivity analysis and probabilistic risk assessment for geological CO_2 storage.
- Introducing a framework for extensive realistic sensitivity analysis and risk assessment of geological CO_2 storage.

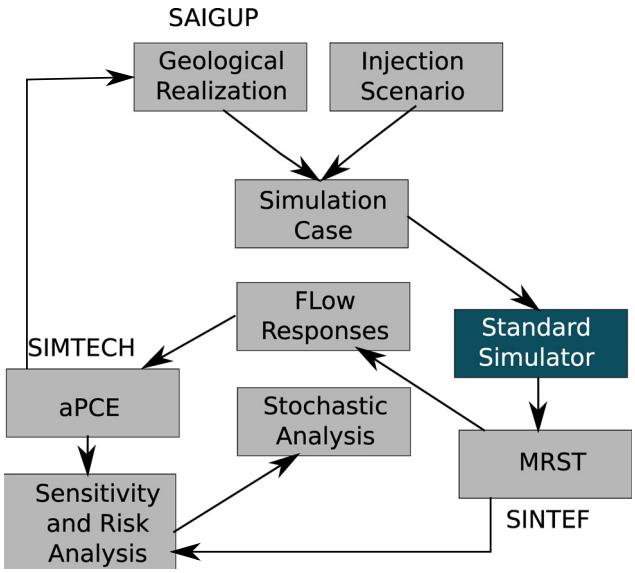

Figure 1.39: Flowchart of workflow implemented in an automated procedure.

The significance of geological uncertainty is examined through an extensive study of CO_2 flow in different geological models. Sensitivity analysis and risk assessment provided a ranking of the studied geological parameters for various flow responses in the chosen medium. The workflow implemented in this study is a stepwise procedure that can be generalized for use in any similar large-scale analysis.

1.10.1 Implementation of the work-flow

This thesis incorporated working with a large number of realizations, various flow scenarios, and different procedures and software. While the study was in progress, new ideas and challenges required the manipulation of new steps in the workflow. To achieve the defined goals of the research, an automated workflow was designed that connected different parts of the study. This enhanced the efficiency of performing necessary modifications to the workflow.

The MATLAB programming language is used for implementing the workflow in this research. The main reason for this choice, apart from the rich facilities available within the MATLAB toolboxes, is to utilize the numerous functions within the MATLAB Reservoir Simulation Toolbox (MRST) that is available as free and open-source software. For flow simulations, commercial software is used, which is a standard simulator for the oil and gas industry and research.

Figure 1.39 shows the workflow elements implemented using numerous MATLAB functions. Functions from MRST at SINTEF and the stochastic tools from the SIMTECH group at Stuttgart University are utilized and merged into the workflow. The workflow design is constructed to be flexible and general. Some research at SINTEF has been performed by replacing the commercial simulator with in-house simulators. However, the main study is performed using a commercial standard simulator.

1.10.2 Generic application of results

We rank the most influential geological parameters for early stages of CO_2 storage operations. The demonstrated workflow can be used in any study concerning the site selection and early stages of geological CO_2 storage. However, there are some limitations in our presentation of the workflow that must be considered when this work is applied in similar studies.

The first limitation is the SAIGUP model size. CO_2 storage studies require large models that can cover the CO_2 spatial traveling extent within the aquifer. Therefore, our study is limited to the domain around the injector.

An over-pressurized injection can introduce breakings in the sealing cap-rock that is used for structural CO_2 trapping. It is more feasible to use a minimum number of wells to minimize the project costs and the risk of CO_2 leakage through abandoned wells. Therefore, a typical injection scenario includes a few injectors with no production well to balance the injection pressure. The elliptic nature of the pressure equation and the small compressibility of the medium produce a large area influenced by the injection pressure. Therefore, pressure-related studies require a large model domain to study the effect of the impulse imposed by the injector on the entire region connected to the impulse.

To overcome this limitation in the SAIGUP models, we exaggerated the cell volumes at the model boundaries that are supposed to be open. The large pore volumes on the boundaries avoid extreme pressure build-up caused by injecting into a closed system. However, the study is limited to the region near the well. Because the high pressures occur near the injector, it is more interesting to study pressure build-up around the well rather than examining the entire region influenced by the injection pressure.

The pressure behavior is very sensitive to the way the boundaries are defined. In reality, there are different aquifer systems. Some aquifers are large with very large pore volumes. To model these aquifers, we can use smaller model domains with open boundaries. However, some aquifers are medium and small in size. To model these aquifers, we can assume semi-closed and closed boundaries. For any aquifer system, we can define the boundary by exaggerating the pore volume of the cells along the model boundaries. The transmissibilities of the boundary cells can also be modified to represent the size of the aquifer system, controlling the amount of pressure relaxation in the medium through the boundaries. If CO_2 exists in the boundaries, relative permeability function at the boundary can be modified in addition to the transmissibilities.

The open boundaries in our study are considered completely open. This assumption allows pressure to relax through the boundaries. However, the results of our pressure study are influenced by this choice. While we have observed a many cases with extreme pressures due to heterogeneity effects, the pressures reported in our study are moderate compared to partially closed boundaries. The sensitivity analysis is based on comparing the pressure values of the different cases. Therefore, the outcome of the sensitivity analysis should be valid regardless of the boundary choices. The size limitation in the SAIGUP models resulted in an extension to the current study, which is called IGEMS [67].

The IGEMS models are larger compared to the SAIGUP models. There is only one major structural trap in the SAIGUP models that allows for most of the injected CO_2 to accumulate under the cap-rock. This is not sufficient for studying the effect of variations in the top-surface topography on CO_2 movement in the medium. The IGEMS study has focused on the structural trapping due to deformations in the top-surface morphology and faults. The results show that structural trapping can be important in controlling the extent of CO_2 storage due to structural trapping and controlling the speed of the plume migrating under the top sealing cap-rock.

In the vertical direction, the SAIGUP models can be improved with a higher grid resolution. Variations in the vertical direction exist at considerably smaller scales than in the horizontal. In particular, this is more important for the long-term CO_2 migration in which a thin plume of CO_2 migrates beneath a sealing layer due to buoyancy forces.

Another issue to be mentioned is the geological uncertainty assumption used in the stochastic analysis. We consider nearly uniform distributions for the probabilities of uncertain parameter values. While there is no loss of generality, there are two comments that could improve our analysis:

- In general, the uncertainty probability may not directly follow a uniform distribution. Actually, this information is very case dependent and can change from one location to another.

- One advantage of the aPC method is its flexibility to be applied for arbitrary forms of uncertainty data. Choosing various distributions for the geological parameters would better demonstrate the strength of the aPC method.

Because we are limited to the SAIGUP models that are based on equally probably values for the geological parameters, uniform uncertainty distributions are chosen. A general stochastic process using the aPC must be considered in the following steps:

- Use the techniques from the aPC method to derive appropriate sample points for the geological parameters.
- Construct geological models at these sample points.
- Perform flow simulations for each sample point.
- Construct the proxy model.
- Perform global sensitivity analysis using the Sobol indexes method and the proxy model.
- Perform the Monte Carlo simulations using the aPC study to assess the uncertainty and risk.

The link between designing geological realizations and the implementation of the aPCE method is depicted in Figure 1.39. The sensitivity analysis and risk assessment procedure must start from the 'aPCE' box in Figure 1.39. The collocation points from the given geological uncertainty are first found, and then, based on those collocation points, we design the geological realizations. However, due to the availability of a large set of SAIGUP realizations generated before this study, our starting point was from the 'Geological Realization' box in Figure 1.39. This change resulted in assuming a given geological uncertainty knowledge that suits the SAIGUP geological design. Nevertheless, we practice the procedure in a geological modeling and flow analysis scope that is novel and can be consulted for further extensive studies.

Chapter 2

Introduction to the papers

2.1 Introduction

The main scientific part of this thesis consists of three papers. They come in a sequence to show the research progress within this PhD program. Paper I includes a detailed study of how variations in geological parameters impact the evolution of the injected CO_2 plume. Knowing the migration path of the plume is essential if one wants to assess the risk for CO_2 leaving the aquifer through imperfections in the caprock or through open lateral boundaries. Second, to determine the fasibility of the injection process and reduce the potential for introducing fracturing during the injection process, it is crucial to know the pressure buildup. Likewise, it is important to know how far pressure pulses induced during injection propagate beyond the zones invaded by the injected CO_2. Therefore, a special study is dedicated to pressure analysis in the system. This is reported in Paper II, which is submitted to the International Journal of Greenhouse Gas Control (IJGGC). Finally, Paper III reports modern stochastic techniques used to perform detailed quantitative sensitivity analysis and probabilistic risk assessments. This paper is accepted for publication in the IJGGC. This paper was submitted for publication earlier than the second paper.

2.2 Summary of papers

Paper I: *Impact of geological heterogeneity on early-stage CO_2 plume migration: CO_2 spatial distribution sensitivity study*

Summary:

We use a set of SAIGUP realizations selected to cover the variability of five sedimentological and structural geological parameters. The selected parameters are lobosity, barriers, aggradation angle, progradation direction, and faults. Each of these parameters varies over three levels, except the progradation direction, which includes up-dip and down-dip directions. Combining the available parameters makes 162 realizations. However, two cases were missing in the original setup. Therefor, 160 geological realizations are used here.

30 years of injection and 70 years of early migration of CO_2 are simulated and flow responses related to the storage capacity and leakage risk objectives are defined and calculated from the simulation results. The responses are reported in scatter plots at the end of injection and at the end of early migration time.

This work is specific in examining how heterogeneity influences flow behavior by using a number of geological realizations. Flow responses defined in this work are specific to CO_2 studies and differ from the responses used in the original SAIGUP project to study oil recovery. We simulate the aquifer average pressure, residual and mobile CO_2 saturation, and spatial distribution of connected CO_2 volumes. These responses can be considered to evaluate the site storage capacity and risk of CO_2 leakage to surface.

The injector is controlled by a constant rate and no pressure constraint is set to allow for all ranges of pressure, including those that are unrealistic. Moreover, we define an additional model output that is related to the risk of CO_2 leakage through any breakings in the cap-rock.

Finally, we perform a quantitative sensitivity analysis by using the flow simulation results. The sensitivity analysis results suggest that aggradation angle, fault criteria, and progradation direction are the most influential geological parameter in our study.

In this work, we clearly see the range of variations in the flow responses that demonstrates how important it is to model the geological features accurately.

Comments: This work initially was presented at the ACM conference in Edinburgh, 2010. More details of the work are reported in proceedings for the CMWR conference in Barcelona, 2010 and in the ECMOR conference in Oxford, 2010. The final version is submitted to the Goundwater.

The following comments are important to be considered here:

- *The SAIGUP realizations*

  Topography is a major player in the gravity dominated flow behavior. The SAIGUP realizations include variability in topography of the geological layering via structural changes due to faults and also barriers in the model. These are good enough for early migration when the CO_2 and water segregate and plumes accumulate below cap-rock and start the longer migration. In the long-term migration, top surface geometry is an important geological parameter and larger models than the SAIGUP models with a better resolution of the top surface are needed to get good predictions of the long-term migration phase. This was considered in the next generation of geological studies performed following this study [53, 67] under the IGEMS research project.

- *Physical assumptions*

  The work concentrates on how geological heterogeneity impacts the flow performance. We need to measure the volumetric sweep efficiency of CO_2 plumes to evaluate the residual trapping. Including more physics in the modeling will add the computational costs specially when the flow modeling is used in a sensitivity analysis or risk assessment process. Therefore, we used simple fluid models for PVT.

- *Uncertainty considerations*

  Our main motivation for using the SAIGUP data was the extensive work that was put into building realistic geological realizations. The geological parameters are changed in value between low and high levels. These values are assumed with the same probability. In general, this probability might not be uniform, depending to the regional geology of the storage site.

Within one geological realization, injection location can dramatically impact the injectivity of the well. In fact, this is an uncertain parameter in the CO_2 storage operations. Choosing to inject in the river channels or in the permeable homogeneous parts near the shore will enhance the injectivity and the CO_2 sweep efficiency in the medium. On the other hand, injecting in locations with low permeabilities and pore-volumes can significantly increase the injection pressure, while limiting the transport of CO_2 in the medium. Studying the impact of injection location can be performed by injecting in many different points in one realization and comparing the corresponding flow responses. However, this will considerably increase the number of detailed simulations in the study.

For the allowed time, we limited our study to a fixed point by injecting via one well in the flank part of the SAIGUP models. This location is selected after qualitative analysis of a detailed study on a homogeneous case. There, we aimed to fulfill the criterion of maximizing the CO_2 storage capacity via increasing the vertical travel path toward the structural trap location under the cap-rock. One mitigating strategy for minimizing the effect of injection location can be to inject via several wells in different locations in the medium.

Similar argument applies to the leakage risk study reported here. We use a leakage probability over the cap-rock that can dramatically influence the calculated leakage risk. We take this assumption to simplify the way we introduce the method.

Contribution of the candidate:

The idea of using realizations from the SAIGUP project to study how variations in geological parameters impact the injection and early-stage migration of CO2 was first suggested by the main supervisor of this thesis. The conceptual design of the injection scenario, as well as the measured reservoir responses were developed jointly with the co-authors of the paper. The candidate was solely responsible for working out the details of the simulation setup, developing a work-flow, performing simulations, post-processing results, and developing the first analysis of the results. The candidate then collaborated with the co-authors to refine the analysis and write the paper.

Paper II: *Geological storage of CO_2: heterogeneity impact on pressure behavior*

Summary:

Pressure build-up is an important criterion that can determine the success and failure of CO_2 storage operations. Over-pressurized injections can induce new fractures and open the existing faults and fractures that increases the risk of leakage for the mobile CO_2 in the domain. On the other hand, the pressure disturbance imposed on the system travels within the domain beyond the scales of CO_2 distribution. If the CO_2 is injected into a saline aquifer connected to fresh water aquifers, the pressure pulse may result in fresh water contaminations by the brine far from the injection point. We define specific pressure responses to examine the pressure disturbance in the system during injection.

Two injection scenarios are examined for the same 160 geological realizations setup. In the first scenario, the injector is set to a fixed volumetric rate to inject the CO_2 volume in 30 years into the domain, allowing for an unlimited pressure build-up. In the second scenario, a pressure constraint is set on the injector that results in various rate of injection in different geological realizations to inject the same amount of CO_2 volume considered in the first injection scenario.

Pressure response sensitivity study with respect to different geological features indicates the significance of aggradation angle, progradation direction, and faults during injection. A probabilistic pressure analysis is also performed based on the 160 simulations on the available realizations.

Comments:

The results reported in this paper can vary by choosing different boundary conditions for the model and different model size. We choose open boundaries on three sides of the model. In general, pressure values can be larger than those that are simulated here.

Well location is chosen to be fixed in our study. Choosing different location of injection in the model can result in a dramatically different pressure behavior. We use one injector in the study to simplify the pressure analysis. To investigate the effect of well location on the results, one can inject via many injectors. Other option is to study the impact of changing the well location in a single injector model.

Finally, the early pressure build up that happens around the well is due to the low CO_2 saturations existing near the injector in the beginning of injection. This build-up is sensitive to the grid resolution around the injector. The simulated pressures can be less if we use finer grid near the injector. In some experiments that is not reported in the paper, we concluded that, with the grid used in our study, this difference is not very dramatic.

Paper III: *Geological storage of CO_2: global sensitivity analysis and risk assessment using the arbitrary polynomial chaos expansion*

Summary:

In this paper, we perform a stochastic sensitivity and risk analysis. We obtain a high resolution global sensitivity and probabilistic study on the flow responses that are defined and discussed in the previous papers. We choose barriers, aggradation angle, and faults from the SAIGUP geological parameters. Faults are considered by changing the transmissibility value across them, which is a continuous parameter. One more parameter is added to the study which is common in the literature and models the external pressure support from other aquifers attached to the model (regional groundwater effect).

Flow simulation on high resolution variational geology demands a huge computational costs. To enhance the calculation speed, we use a data-driven method that does not need to solve the full physical flow equations. We approximate the flow solver by a response surface method that is a polynomial and relates the system output to the input with a minimal computational cost. We use the arbitrary polynomial chaos expansion (aPC) to approximate the flow responses. The aPC method considers the uncertainty in the input variables.

A global sensitivity analysis is performed by employing Sobol indices that are based on variances of responses. The method is shown to be robust in problems of high levels of complexity and non-linearity.

And finally, we perform a Monte-Carlo process using the approximating polynomial on a high

resolution input variations. This makes it possible to perform a high resolution probabilistic study on the flow responses. This way, extreme cases can be identified by probability of occurrence.

Comments:

This work was presented in the proceedings of the European Geosciences Union (EGU) General Assembly 2012, April, Vienna, Austria, Geophysical Research Abstracts., Vol. 14, EGU2012-9243. The detailed report is accepted for publication in the International Journal of Greenhouse Gas Control (IJGGC), in May 2013, http://dx.doi.org/10.1016/j.ijggc.2013.03.023.

To implement our stochastic technique, we choose geological parameters in this study that can be interpolated between two levels of their values. For example, it makes sense to use barriers coverage level of 25% between the low (10%) and medium (50%) levels used in the previous studies. Some of the geological parameters are discrete and can not be interpolated between two values. For instance, lobosity can only be varied over three points and we can not define a 1.5-lobe.

Having a large number of points in the input values interval requires intensive geological modelings to be used in the flow simulations. Using the data-driven polynomial, the approach only needs evaluating the polynomial in the defined values, and there is no need for full geological modeling except in the collocation points, i.e., point values that the polynomial coefficients must be calculated.

The work reported here is to demonstrate the work-flow of using the aPC for global sensitivity analysis and probabilistic risk assessment. A normal work-flow starts by defining the uncertainties in the input parameters and follows by building the geological models for the aPC collocation points that are based on those uncertainties. To perform this study on the SAIGUP models that are consistent with a uniform uncertainty in the geological parameters, with no loss of generality, we used uniform uncertainty distributions for our study. However, the aPC method is not limited to uniform uncertainty descriptions.

Geological features are ranked based on the sensitivity analysis results. The results are in agreement with dynamics of the flow in the aquifer. Aggradation angle is the most influential parameter, while the regional groundwater has the least influence in the model responses. The study is not limited to the assumed uncertainty of input parameters and the conclusion may change for a very different uncertainty description.

Contribution of the candidate:

The study was a joint work between the candidate and the co-authors on the following steps:

- Defining the problem.
- Designing the simulation scenarios.
- Designing the work-flow.
- Integrating the aPC MATLAB code into the work-flow.
- Performing the runs and processing the results.
- Performing the global sensitivity analysis.
- Performing the risk assessment.
- Analyzing the results and preparing plots.
- Writing the report.

The candidate had a solid and major contribution in every step, and in particular, integrating the aPC code into the work-flow, running the simulations, performing the sensitivity and risk analysis, and processing the results. The report has gone through extensive reviews.